IEEE Access
Multidisciplinary | Rapid Review | Open Access Journal

Received February 11, 2020, accepted February 24, 2020, date of publication February 27, 2020, date of current version March 12, 2020.

Digital Object Identifier 10.1109/ACCESS.2020.2976698

Self-Healing Control for Large Launch Vehicle Based on Extended State Observer and Adaptive Dynamic Programming

XIAOHUI LIANG[1], QING WANG[1], CHANGHUA HU[2], ZHIJIE ZHOU[2], AND CONG FENG[1]
[1]School of Automation Science and Electrical Engineering, Beihang University, Beijing 100191, China
[2]Department of Automation, High-Tech Institute of Xi'an, Xi'an 710025, China

Corresponding author: Xiaohui Liang (liangxiaohui@buaa.edu.cn)

This work was supported in part by the National Nature Science Foundation of China under Grant 61873295, Grant 61833016, Grant 61622308, and Grant 61933010.

ABSTRACT This paper investigates the self-healing control problem for the large launch vehicle (LLV) with system uncertainties, external disturbances, and actuator faults. First, the attitude dynamics of the LLV are presented, and the control-oriented model subject to undesired malfunctions is structured. Second, a novel extended state observer (ESO) is designed to estimate the disturbances and fault informations, and the nonlinear gain functions with two different linear ranges are introduced to improve the estimation accuracy and reduce the effect of peaking value problem. Then, an integral terminal sliding mode fault tolerant control scheme is proposed for the attitude faulty system, which would stabilize the closed-loop system even existing the disturbances and actuator failures. Besides, utilizing the adaptive dynamic programming (ADP) technique, a supplementary control with actor-critic structure is employed to further improve the system tracking performance and provide the additional compensation control input according to the bias between the desired value and actual one. Finally, the effectiveness of the proposed method is verified by the simulation results.

INDEX TERMS Self-healing control, large launch vehicle, extended state observer, sliding mode control.

I. INTRODUCTION

With the development of the deep space explorations, the large launch vehicles (LLVs) have received extensive attention in aerospace engineering in the past few decades [1]. Different from traditional launch vehicles, the LLV can provide tremendous lift to deliver more payloads to the pre-selected orbit [2], [3]. However, the aerodynamic instability, fuel sloshing, strong nonlinearity and flex-mode have brought great challenges for the design of flight control system [4], [5]. Especially considering the severe flight environment during the ascent phase and complex vehicle structure, it is inevitable that several system or component malfunctions are encountered [6], which may cause the system performance degradation even instability. Therefore, a more safe and reliable control system is required to accommodate undesirable failures.

The associate editor coordinating the review of this manuscript and approving it for publication was Nasim Ullah.

The self-healing control technique is an effective method to counteract system malfunctions and maintain control performance with an acceptable degree, and many research results on the self-healing control have been obtained [7], [8]. Among these optional self-healing control approaches, the passive fault tolerant control and active fault tolerant control are the most common control techniques [9]. The fixed control structure is usually utilized to be robust against the given faults in the passive tolerant control. Thus, passive tolerant control method can be regarded as a special form of the robust control [10]. Considering the external disturbances and unknown actuator loss of effectiveness, the passive fault tolerant control approach is proposed in [11] for the hypersonic vehicle by the terminal sliding mode technique. In [12], an integral sliding mode fault tolerant control scheme is proposed for the spacecraft attitude system and the adaptive method is applied to remove the restriction for the boundary of faults informations. In [13], a passive fault tolerant attitude stabilization control method is designed, which can guarantee local finite-time stability despite control input saturation.

Although these passive tolerant control methods have relatively simple control structure and not require online fault informations, the fault-tolerant capability is severely limited and only specific types of failures can be handled [14], which serious restrict the application of the passive fault tolerant control.

The active fault tolerant control method makes up for the above shortcomings, which can reconfigure the control parameters and structure based on the online fault estimation informations by the fault diagnosis (FD) mechanism [15]. Thus, a better robustness and fault acceptability can be obtained by the active fault tolerant control, and many related results have been achieved. In the active fault tolerant control design, the detections and estimations of the fault information are crucial issues and plentiful approaches are researched. The extended state observer (ESO), as an effective tool to estimate total disturbances [16]–[19], is extensively used during the fault tolerant design process. Considering the actuator faults for the air-breathing hypersonic vehicle, Liu *et al.* [20] developed an ESO-based back-stepping fault tolerant control scheme for the attitude system, and two ESOs are applied in each step, where the first ESO is used to approximate the virtual control command and the second one estimates the unknown disturbances, uncertainties and actuator faults simultaneously. In [21], a fixed-time extended state observer is proposed to estimate the grid fin faults and system uncertainties for reusable launch vehicle, and an adaptive fault-tolerant control method is developed by the nonsingular fast terminal sliding mode technique, which could guarantee a good tracking performance. For the nonlinear actuator faults and time-varying input delay, the state estimation methods based on the T-S fuzzy approach are proposed in the [22], and non-fragile reliable controller is also designed to ensure the asymptotic stability of the closed-loop systems. The ESO based on the sigmoid function is developed in [23] to estimate the compound disturbances caused by large attitude maneuver and complicated external environment for the reusable launch vehicle. According to the concept of self-healing control method, the fault tolerant control strategy is proposed in the [24] and [25], which integrate the FD and controller in a dynamic system. Combined with the sliding mode and dynamic surface techniques, a self-healing strategy for the hypersonic flight vehicle is proposed in [9] to ensure the stability of the faulty systems. However, the ESO-based self-healing control for large launch vehicle is still an open issue and needs further research, which mainly motivates this study.

On the other hand, most ESO-based fault tolerant control approaches are in absence of the learning and parameter updating capabilities, which would limit the further improving of the system control performance when encountering undesired malfunctions. Different from the traditional control methods, adaptive dynamic programming (ADP) is a data-driven learning technique and independent of the system model and, which has the ability to learn and tune controller parameters online [26]–[28]. In [29], an observer-critic structure-based ADP is proposed to handle the decentralized tracking control problem, and the Hamiltonian-Jacobi-Bellman equation is solved by a critic neural network. A model-free control scheme for a class of nonlinear system is devised in [30] based on an incremental approximate dynamic programming (I-ADP). Combing with ADP and sliding-mode control technique, the tracking control issue is solved in [31] for air-breathing hypersonic vehicles. If there is a discrepancy between the actual value and reference signals, the proposed ADP arithmetic would produce a supplementary control input to improve the system performance. Although, both fault tolerant control and ADP methods have made some achievements, the organic combination of two approaches requires further study.

Motivated by the above discussions, a self-healing control strategy for the large launch vehicle with actuator faults is proposed in this paper. The main contributions of this work can be summarized as follows:

1) Applied with a nonlinear gain function, a novel ESO is proposed to estimate the actuator faults and disturbances, and two different forms of observations are integrated into one ESO, which would avoid the peaking value problem.

2) Based on the estimated informations, an integral terminal sliding mode fault tolerant control scheme is designed for the attitude tracking system of LLV, and the finite time stability of the closed-loop system can be achieved in presence of disturbances and actuator malfunctions.

3) To further improve the system tracking performance, an ADP with actor-critic structure is employed in the supplementary controller, which would learn and tune controller parameters according to the bias between the actual value and the desired one.

The remainders of this paper are organized as follows: Section II introduces the attitude dynamics of the LLV and the control-oriented modes with actuator faults are established. The ESO and fault tolerant control schemes are proposed in Section III, and the design of supplementary controller based on ADP is also described in this section. Furthermore, the simulation results are presented in Section IV. Finally, Section V provides a discussion of conclusions.

Notation: $\mathbb{R}^n$ is the n-dimensional Euclidean space, and $||\cdot||$ refers to the Euclidean vector norm. $\boldsymbol{I}_n$ denotes the n-dimensional identity matrix. For a matrix $\boldsymbol{Q} \in \mathbb{R}^{m\times n}$, $\boldsymbol{Q}^{\mathrm{T}}$ and $\boldsymbol{Q}^{-1}$ are the transposition and inverse of $\boldsymbol{Q}$, respectively. The $\lambda_{\min}(\boldsymbol{Q})$ represents the minimum eigenvalue of the matrix $\boldsymbol{Q}$, and $\boldsymbol{x}^{\times}$ stands for the skew-symmetric matrix corresponding to the vector $\boldsymbol{x} = [x_1, x_2, x_3]^{\mathrm{T}} \in \mathbb{R}^3$. Furthermore, $\mathrm{sat}(\cdot)$ and $\mathrm{sgn}(\cdot)$ represent the standard saturation function and sign function, respectively.

II. DYNAMIC MODEL AND PROBLEM FORMULATION

In this section, the attitude dynamics of the large launch vehicle is first introduced, and the control-oriented models with actuator malfunctions are constructed. Besides, the main objective of this note is also formulated in this section.

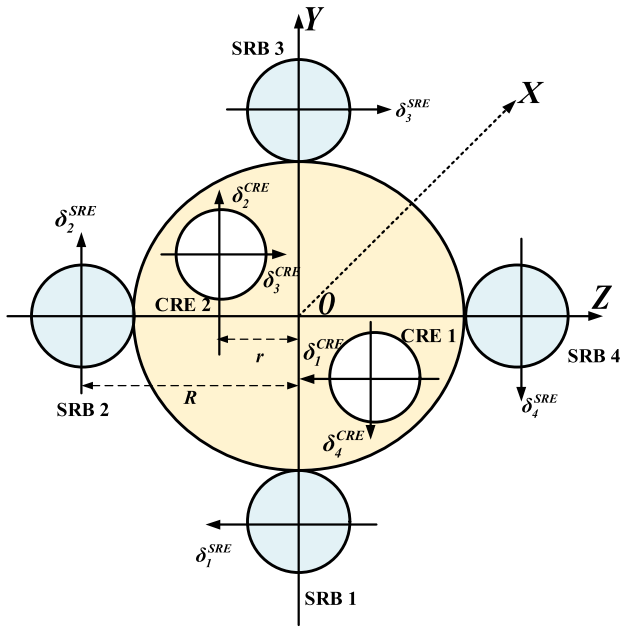

FIGURE 1. The configuration of propulsive engines.

A. ATTITUDE DYNAMICS OF LLV

A class of large launch vehicles (LLV) is considered in this paper, and the propulsion system of the LLV is constituted by two central rocket engines (CREs) and four strap-on rocket boosters (SRBs), which would provide the control torques for three channels, i.e. the pitch, yaw and roll channel [2]. The main control objective of this note is to design a self-healing control strategy for attitude dynamics of the LLV with actuator failures, so the rotational equation is only expressed in this paper, more information for the LLV mode can be found in [6] and [21]. The dynamic model of the rotational motion for LLV is given as follows:

$$\boldsymbol{J}\dot{\boldsymbol{\omega}} = -\boldsymbol{\omega}^{\times}\boldsymbol{J}\boldsymbol{\omega} + \boldsymbol{\tau} + \boldsymbol{d} \tag{1}$$

where $\boldsymbol{\tau} \in \mathbb{R}^3$ is the control torque vector, $\boldsymbol{d} = \left[d_x, d_y, d_z\right]^{\mathrm{T}}$ is the unknown external disturbances, $\boldsymbol{J} = \mathrm{diag}\left(J_{xx}, J_{yy}, J_{zz}\right)^{\mathrm{T}} \in \mathbb{R}^{3\times3}$ denotes the moment of inertia for the axisymmetrical structure LLV, $\boldsymbol{\omega} = \left[\omega_x, \omega_y, \omega_z\right]^{\mathrm{T}} \in \mathbb{R}^3$ represents the inertial angular velocity vector of the LLV with respect to an inertial frame y, and $\boldsymbol{\omega}^{\times}$ stands for the skew-symmetric matrix operator, which can be expressed as

$$\boldsymbol{\omega}^{\times} = \begin{bmatrix} 0 & -\omega_z & \omega_y \\ \omega_z & 0 & -\omega_x \\ -\omega_y & \omega_x & 0 \end{bmatrix}$$

The configuration of the propulsive rocket engines for LLV is presented in Fig. 1. Arrows denote the positive directions of engine, and it can be found that four SRBs can only move in one axis, while two CREs can move in two axes [6]. Note that the control torque for the pitch channel can be provided by the 2−th SRB and 4-th SRB, for the yaw channel can be offered by the 1-th SRB and 3-th SRB. Two CREs can contribute the control torques for both pith and yaw channels. Specially, the control torque for the roll channel is generated by all engines.

Thus, the equivalent deflection angle $\boldsymbol{\delta} = \left[\delta_x, \delta_y, \delta_z\right]^{\mathrm{T}}$ for three channels can be described by

$$\boldsymbol{\delta} = \boldsymbol{T}_{\mathrm{CRE}}\boldsymbol{\delta}^{\mathrm{CRE}} + \boldsymbol{T}_{\mathrm{SRE}}\boldsymbol{\delta}^{\mathrm{SRE}} \tag{2}$$

where $\boldsymbol{\delta}^{\mathrm{CRE}} = \left[\delta_1^{\mathrm{CRE}}, \delta_2^{\mathrm{CRE}}, \delta_3^{\mathrm{CRE}}, \delta_4^{\mathrm{CRE}}\right]^{\mathrm{T}} \in \mathbb{R}^4$ and $\boldsymbol{\delta}^{\mathrm{SRE}} = \left[\delta_1^{\mathrm{SRE}}, \delta_2^{\mathrm{SRE}}, \delta_3^{\mathrm{SRE}}, \delta_4^{\mathrm{SRE}}\right]^{\mathrm{T}} \in \mathbb{R}^4$ represent the deflection angles of SRBs and CREs, respectively. The $\boldsymbol{T}_{\mathrm{CRE}}, \boldsymbol{T}_{\mathrm{SRE}} \in \mathbb{R}^{3\times4}$ are the distribution matrices, and their forms are given as follows

$$\boldsymbol{T}_{\mathrm{CRE}} = \begin{bmatrix} 1/2 & 1/2 & 1/2 & 1/2 \\ 0 & -1 & 0 & 1 \\ -1 & 0 & 1 & 0 \end{bmatrix}$$

and

$$\boldsymbol{T}_{\mathrm{SRE}} = \begin{bmatrix} 1/4 & 1/4 & 1/4 & 1/4 \\ 0 & -1/2 & 0 & 1/2 \\ -1/2 & 0 & -1/2 & 0 \end{bmatrix}.$$

Then, the control torque $\boldsymbol{\tau}$ can be obtained

$$\boldsymbol{\tau} = \boldsymbol{G}\boldsymbol{\delta} = \begin{bmatrix} -T\,(4R + r)\,\delta_x \\ -\dfrac{5}{2}T(L - x_m)\delta_y \\ -\dfrac{5}{2}T(L - x_m)\delta_z \end{bmatrix} \tag{3}$$

where diagonal matrix $\boldsymbol{G} \in \mathbb{R}^{3\times3}$ is the moment conversion matrix, R and r denote the distances from x-axis to the SRB and to CRE, respectively. x_m stands for the location of mass center, L denotes the distance from the engine to the top of the rocket, and T represents the thrust magnitude. More informations about the LLV can be found in [2] and [6].

According to the transformational from the inertial frame to body frame, the attitude dynamics can be obtained as follows

$$\begin{aligned} \dot{\boldsymbol{\xi}} &= \begin{bmatrix} \dot{\phi} \\ \dot{\psi} \\ \dot{\theta} \end{bmatrix} = \boldsymbol{S}\left(\boldsymbol{\xi}\right)\boldsymbol{\omega} \\ &= \begin{bmatrix} 1 & \tan\psi\sin\phi & \tan\psi\cos\phi \\ 0 & \cos\phi & -\sin\phi \\ 0 & \sec\psi\sin\phi & -\sec\psi\cos\phi \end{bmatrix} \begin{bmatrix} \omega_x \\ \omega_y \\ \omega_z \end{bmatrix} \end{aligned} \tag{4}$$

where the attitude vector $\boldsymbol{\xi} = [\phi, \psi, \theta]^{\mathrm{T}} \in \mathbb{R}^3$, ϕ, ψ and θ represent roll angle, yaw angle, and pitch angle, respectively.

B. PROBLEM FORMULATION

The gain and bias faults are considered for CREs and SREs in this paper, which commonly occurs on the actuator system [34]. And the actuator fault model including both sorts of faults is generally formed as

$$\begin{cases} \boldsymbol{\delta}_f^{\mathrm{CRE}} = \boldsymbol{E}^{\mathrm{CRE}}\boldsymbol{\delta}^{\mathrm{CRE}} + \boldsymbol{\rho}^{\mathrm{CRE}}, \\ \boldsymbol{\delta}_f^{\mathrm{SRE}} = \boldsymbol{E}^{\mathrm{SRE}}\boldsymbol{\delta}^{\mathrm{SRE}} + \boldsymbol{\rho}^{\mathrm{SRE}}, \end{cases} \tag{5}$$

where $\boldsymbol{E}^{\mathrm{CRE}} = \mathrm{diag}\left(e_1^{\mathrm{CRE}}, e_2^{\mathrm{CRE}}, e_3^{\mathrm{CRE}}, e_4^{\mathrm{CRE}}\right)$ and $\boldsymbol{E}^{\mathrm{SER}} = \mathrm{diag}\left(e_1^{\mathrm{SRE}}, e_2^{\mathrm{SRE}}, e_3^{\mathrm{SRE}}, e_4^{\mathrm{SRE}}\right)$ represent actuator effectiveness, such that $0 < e_i^{\mathrm{CRE}} \leq 1, 0 < e_i^{\mathrm{SRE}} \leq 1\,(i = 1, 2, 3, 4)$, $\boldsymbol{\rho}^{\mathrm{CRE}} = \left[\rho_1^{\mathrm{CRE}}, \rho_2^{\mathrm{CRE}}, \rho_3^{\mathrm{CRE}}, \rho_4^{\mathrm{CRE}}\right]^{\mathrm{T}}$ and $\boldsymbol{\rho}^{\mathrm{SRE}} = \left[\rho_1^{\mathrm{SRE}}, \rho_2^{\mathrm{SRE}}\ \rho_3^{\mathrm{SRE}}, \rho_4^{\mathrm{SRE}}\right]^{\mathrm{T}}$ are the bias faults. Therefore, the actual control torques $\boldsymbol{\tau}_f = \boldsymbol{G}\boldsymbol{\delta}_f = \boldsymbol{T}_{\mathrm{CRE}}\boldsymbol{\delta}_f^{\mathrm{CRE}} + \boldsymbol{T}_{\mathrm{SRE}}\boldsymbol{\delta}_f^{\mathrm{SRE}}$, where $\boldsymbol{\tau}_f \in \mathbb{R}^3$ and $\boldsymbol{\delta}^f = \left[\delta_x^f, \delta_y^f, \delta_z^f\right]^{\mathrm{T}} \in \mathbb{R}^3$.

According to (1)-(5), the attitude system with actuator faults for the LLV can be rewritten as

$$\begin{cases} \dot{\boldsymbol{\xi}} = \boldsymbol{S}(\boldsymbol{\xi})\,\boldsymbol{\omega}, \\ \dot{\boldsymbol{\omega}} = \boldsymbol{J}^{-1}\left(-\boldsymbol{\omega}^{\times}\boldsymbol{J}\boldsymbol{\omega} + \boldsymbol{\tau}_f + \boldsymbol{d}\right) \\ = -\boldsymbol{J}^{-1}\boldsymbol{\omega}^{\times}\boldsymbol{J}\boldsymbol{\omega} + \boldsymbol{J}^{-1}\boldsymbol{G}\left(\boldsymbol{E}\boldsymbol{\delta} + \boldsymbol{\rho}\right) + \boldsymbol{J}^{-1}\boldsymbol{d}. \end{cases} \tag{6}$$

Define tracking errors as $\boldsymbol{e}_1 = \boldsymbol{\xi} - \boldsymbol{\xi}_c$ and $\boldsymbol{e}_2 = \dot{\boldsymbol{\xi}} - \dot{\boldsymbol{\xi}}_c$, where $\boldsymbol{\xi}_c$ and $\dot{\boldsymbol{\xi}}_c$ denote the command attitude vector and its derivative, respectively. Then, the following attitude tracking error system is given

$$\begin{cases} \dot{\boldsymbol{e}}_1 = \boldsymbol{e}_2, \\ \dot{\boldsymbol{e}}_2 = \dot{\boldsymbol{S}}(\boldsymbol{\xi})\,\boldsymbol{\omega} + \boldsymbol{S}(\boldsymbol{\xi})\,\dot{\boldsymbol{\omega}} - \ddot{\boldsymbol{\xi}}_c \\ = \left(\dot{\boldsymbol{S}} - \boldsymbol{S}\boldsymbol{J}^{-1}\boldsymbol{\omega}^{\times}\boldsymbol{J}\boldsymbol{\omega}\right)\boldsymbol{\omega} + \boldsymbol{S}\boldsymbol{J}^{-1}\boldsymbol{G}\left(\boldsymbol{E}\boldsymbol{\delta} + \boldsymbol{\rho}\right) + \boldsymbol{S}\boldsymbol{J}^{-1}\boldsymbol{d} - \ddot{\boldsymbol{\xi}}_c. \end{cases} \tag{7}$$

In order to describe simply, the (7) can be rewritten as

$$\begin{cases} \dot{\boldsymbol{e}}_1 = \boldsymbol{e}_2, \\ \dot{\boldsymbol{e}}_2 = \boldsymbol{F}\boldsymbol{\omega} + \boldsymbol{G}_1\boldsymbol{\delta} + \boldsymbol{D} - \ddot{\boldsymbol{\xi}}_c. \end{cases} \tag{8}$$

where $\boldsymbol{F} = \dot{\boldsymbol{S}} - \boldsymbol{S}\boldsymbol{J}^{-1}\boldsymbol{\omega}^{\times}\boldsymbol{J}\boldsymbol{\omega}, \boldsymbol{G}_1 = \boldsymbol{S}(\boldsymbol{\xi})\boldsymbol{J}^{-1}\boldsymbol{G}$ and $\boldsymbol{D} = \boldsymbol{S}\boldsymbol{J}^{-1} \cdot \{\boldsymbol{G}\left[(\boldsymbol{E} - \boldsymbol{I})\,\boldsymbol{\delta} + \boldsymbol{\rho}\right] + \boldsymbol{d}\}$. Therefore, the control-oriented attitude tracking models with actuator faults for the LLV are established.

The main control objective of this note is to design an FTC strategy for attitude dynamics of the LLV, which would make the attitude angle track the given command with a good performance even in the presence of uncertainties, external disturbances and actuator faults simultaneously.

Assumption 1: The compound disturbance $\boldsymbol{D}$ in (8) is bounded and differentiable, i.e., there exist positive constants d_1 and d_2, such that $\|\boldsymbol{D}\| \leq d_1$ and $\left\|\dot{\boldsymbol{D}}\right\| \leq d_2$.

Remark 1: The deflection angles of aerodynamic surface and engines are continuous and bounded within certain ranges. Thus, the additional aerodynamic uncertainties and disturbances are also bounded. Moreover, it is reasonable for the engineering practice to assume that the actuator faults and external disturbances are bounded. The similar assumption could be found in [9].

III. MAIN RESULTS

In this section, the self-healing control strategy for LLV is proposed to stable attitude tracking systems. In order to estimate malfunction informations and external disturbances, an extended state observer is first constructed. Then, employed the sliding mode technique, an ESO-based fault tolerant controller is proposed to ensure the stability of the closed-loop system. Finally, an adaptive dynamics programming tool is used to improve the tracking performance.

A. ESO DESIGN

To estimation the compound disturbance $\boldsymbol{D}$ in (8), which includes fault signals and system uncertainties. The following extended state observer is designed

$$\begin{cases} \dot{\tilde{\boldsymbol{e}}}_2 = \boldsymbol{F}\boldsymbol{\omega} + \boldsymbol{G}_1\boldsymbol{\delta} + \tilde{\boldsymbol{D}} - \ddot{\boldsymbol{\xi}}_c + r_1\left[\frac{1}{\mu_1}\left(\boldsymbol{e}_2 - \tilde{\boldsymbol{e}}_2\right) + \frac{r_3\left(\mu_1 - \mu_2\right)}{\mu_2}\right. \\ \left.\cdot\ \mathrm{sat}\left(\frac{1}{\mu_1 r_3}\left(\boldsymbol{e}_2 - \tilde{\boldsymbol{e}}_2\right)\right)\right], \\ \dot{\tilde{\boldsymbol{D}}} = r_2\left[\frac{1}{\mu_1^2}\left(\boldsymbol{e}_2 - \tilde{\boldsymbol{e}}_2\right) + \frac{r_3\left(\mu_1^2 - \mu_2^2\right)}{\mu_1\mu_2^2}\mathrm{sat}\left(\frac{1}{\mu_1 r_3}\left(\boldsymbol{e}_2 - \tilde{\boldsymbol{e}}_2\right)\right)\right], \end{cases} \tag{9}$$

where $\tilde{\boldsymbol{e}}_2 \in \mathbb{R}^3$ and $\tilde{\boldsymbol{D}} \in \mathbb{R}^3$ denote the observer states, r_i, $(i = 1, 2, 3)$ and $\mu_j, (j = 1, 2)$ are observer gains to be determined later.

According to the proposed ESO (9), the following theorem can be obtained.

Theorem 1: Consider the attitude tracking error system (8) and the ESO (9) under the Assumption 1, if the observer gains r_i, $(i = 1, 2, 3)$ and μ_j, $(j = 1, 2)$ are positive constants, such that $\mu_2 < \mu_1 \ll 1$, then the estimation errors would converge to some small residual set of zero, i.e. $\|\boldsymbol{e}_2 - \tilde{\boldsymbol{e}}_2\| \to o(\mu_2^2)$ and $\left\|\boldsymbol{D} - \tilde{\boldsymbol{D}}\right\| \to o(\mu_2)$ for $\forall t > t_{\mu_1} + t_{\mu_2}$, where t_{μ_1} and t_{μ_2} are positive scalars corresponding to μ_1 and μ_2, respectively.

Proof: Define the auxiliary variables as: $\boldsymbol{y}_{\mu_1} = \frac{1}{\mu_1}\left(\boldsymbol{e}_2 - \tilde{\boldsymbol{e}}_2\right), \boldsymbol{y}_{\mu_2} = \frac{1}{\mu_2}\left(\boldsymbol{e}_2 - \tilde{\boldsymbol{e}}_2\right), \boldsymbol{y}_D = \boldsymbol{D} - \tilde{\boldsymbol{D}}$, and define the new estimation errors variables as $\boldsymbol{y} = [\boldsymbol{y}_{\mu_1}, \boldsymbol{y}_D]^{\mathrm{T}}, \bar{\boldsymbol{y}} = [\boldsymbol{y}_{\mu_2}, \boldsymbol{y}_D]^{\mathrm{T}}$. Then, taking the derivative of $\boldsymbol{y}_{\mu_1}$ and $\boldsymbol{y}_D$ yields

$$\begin{cases} \dot{\boldsymbol{y}}_{\mu_1} = \frac{1}{\mu_1}\left[\boldsymbol{y}_D - r_1\boldsymbol{y}_{\mu_1} - \frac{r_1 r_3\left(\mu_1 - \mu_2\right)}{\mu_2}\mathrm{sat}\left(\frac{\boldsymbol{y}_{\mu_1}}{r_3}\right)\right], \\ \boldsymbol{y}_D = \dot{\boldsymbol{D}} - \frac{r_2}{\mu_1}\left[\boldsymbol{y}_{\mu_1} + \frac{r_3\left(\mu_1^2 - \mu_2^2\right)}{\mu_2^2}\mathrm{sat}\left(\frac{\boldsymbol{y}_{\mu_1}}{r_3}\right)\right]. \end{cases} \tag{10}$$

Consider the following Lyapunov function candidate as

$$V_1 = \frac{1}{2}\left(\boldsymbol{y}_{\mu_1}^{\mathrm{T}}\boldsymbol{P}_1\boldsymbol{y}_{\mu_1} + \boldsymbol{y}_D^{\mathrm{T}}\boldsymbol{P}_2\boldsymbol{y}_D - 2\boldsymbol{y}_{\mu_1}^{\mathrm{T}}\boldsymbol{P}_3\boldsymbol{y}_D\right) + \lambda\sum_{i=1}^{3}\int_0^{y_{\mu_1}^i}\mathrm{sat}\left(\frac{y_{\mu_1}^i}{r_3}\right)dy_{\mu_1}^i, \tag{11}$$

where constant $\lambda > 0, y_{\mu_1}^i, (i = 1, 2, 3)$ stands for the different elements of the column vector $\boldsymbol{y}_{\mu_1}$. The terms in the first bracket of Eq. (11) are constituted by the observation errors of ESO, which would guarantee the estimation errors converge to some small residual set of zero. According to proposed ESO (9), the saturation function $\mathrm{sat}\left(\frac{1}{\mu_1 r_3}\left(\boldsymbol{e}_2 - \tilde{\boldsymbol{e}}_2\right)\right)$ is

involved, which would synthesize two distinct linear regions in ESO (9). The nonlinear gain function adopted is a combination of two distinct linear regions, which correspond to the transient and steady phase of the disturbance observer, respectively. And $\boldsymbol{P}_i$, $(i = 1, 2, 3)$ represents positive definite symmetric matrices, such that $\boldsymbol{P}_1 - \boldsymbol{P}_3 > 0$ and $\boldsymbol{P}_2 - \boldsymbol{P}_3 > 0$. According to the Young's inequality [38], the following inequality can be obtained

$$\begin{aligned}&\frac{1}{2}\left(\boldsymbol{y}_{\mu_1}^{\mathrm{T}}\boldsymbol{P}_1\boldsymbol{y}_{\mu_1}+\boldsymbol{y}_D^{\mathrm{T}}\boldsymbol{P}_2\boldsymbol{y}_D-2\boldsymbol{y}_{\mu_1}^{\mathrm{T}}\boldsymbol{P}_3\boldsymbol{y}_D\right)\\&\quad\geq\frac{1}{2}\left[\boldsymbol{y}_{\mu_1}^{\mathrm{T}}\left(\boldsymbol{P}_1-\boldsymbol{P}_3\right)\boldsymbol{y}_{\mu_1}+\boldsymbol{y}_D^{\mathrm{T}}\left(\boldsymbol{P}_2-\boldsymbol{P}_3\right)\boldsymbol{y}_D\right]>0.\end{aligned}\tag{12}$$

Furthermore, considering the integral term in (11), the saturation function $\mathrm{sat}\left(y_{\mu_1}^i/r_3\right)$ is an add function for $y_{\mu_1}^i$, which implies that $\lambda\sum_{i=1}^{3}\int_0^{y_{\mu_1}^i}\mathrm{sat}\left(\frac{y_{\mu_1}^i}{r_3}\right)dy_{\mu_1}^i\geq 0$. Therefore, the function V_1 is a positive function, i.e., the choice of the Lyapunov function candidate is reasonable.

Then, taking the time derivative of V_1 along (10) yields

$$\begin{aligned}&\dot{V}_1\\&=\left(\boldsymbol{y}_{\mu_1}^{\mathrm{T}}\boldsymbol{P}_1-\boldsymbol{y}_D^{\mathrm{T}}\boldsymbol{P}_3\right)\dot{\boldsymbol{y}}_{\mu_1}+\left(\boldsymbol{y}_D^{\mathrm{T}}\boldsymbol{P}_2-\boldsymbol{y}_{\mu_1}^{\mathrm{T}}\boldsymbol{P}_3\right)\dot{\boldsymbol{y}}_D\\&\quad+\lambda\sum_{i=1}^{3}\mathrm{sat}\left(\frac{y_{\mu_1}^i}{r_3}\right)\dot{y}_{\mu_1}^i\\&=\frac{\boldsymbol{y}_{\mu_1}^{\mathrm{T}}\boldsymbol{P}_1-\boldsymbol{y}_D^{\mathrm{T}}\boldsymbol{P}_3}{\mu_1}\left[\boldsymbol{y}_D-r_1\boldsymbol{y}_{\mu_1}-\frac{r_1r_3\left(\mu_1-\mu_2\right)}{\mu_2}\mathrm{sat}\left(\frac{\boldsymbol{y}_{\mu_1}}{r_3}\right)\right]\\&\quad+\left(\boldsymbol{y}_D^{\mathrm{T}}\boldsymbol{P}_2-\boldsymbol{y}_{\mu_1}^{\mathrm{T}}\boldsymbol{P}_3\right)\\&\quad\times\left\{\dot{\boldsymbol{D}}-\frac{1}{\mu_1}\left[r_2\boldsymbol{y}_{\mu_1}+\frac{r_2r_3\left(\mu_1^2-\mu_2^2\right)}{\mu_2^2}\mathrm{sat}\left(\frac{\boldsymbol{y}_{\mu_1}}{r_3}\right)\right]\right\}\\&\quad+\frac{\lambda}{\mu_1}\left[\boldsymbol{y}_D^{\mathrm{T}}-r_1\boldsymbol{y}_{\mu_1}^{\mathrm{T}}-\frac{r_1r_3\left(\mu_1-\mu_2\right)}{\mu_2}\mathrm{sat}^{\mathrm{T}}\left(\frac{\boldsymbol{y}_{\mu_1}}{r_3}\right)\right]\mathrm{sat}\left(\frac{\boldsymbol{y}_{\mu_1}}{r_3}\right)\\&=-\frac{\boldsymbol{y}_{\mu_1}^{\mathrm{T}}\left(r_1\boldsymbol{P}_1-r_2\boldsymbol{P}_3\right)\boldsymbol{y}_{\mu_1}}{\mu_1}\\&\quad+\frac{\boldsymbol{y}_{\mu_1}^{\mathrm{T}}\left(\boldsymbol{P}_1-r_2\boldsymbol{P}_2+r_1\boldsymbol{P}_3\right)\boldsymbol{y}_D}{\mu_1}-\frac{\boldsymbol{y}_D^{\mathrm{T}}\boldsymbol{P}_3\boldsymbol{y}_D}{\mu_1}\\&\quad+\frac{r_3}{\mu_1}\boldsymbol{y}_{\mu_1}^{\mathrm{T}}\left[\frac{-r_1\left(\mu_1-\mu_2\right)}{\mu_2}\boldsymbol{P}_1+\frac{r_2\left(\mu_1^2-\mu_2^2\right)}{\mu_2^2}\boldsymbol{P}_3\right]\mathrm{sat}\left(\frac{\boldsymbol{y}_{\mu_1}}{r_3}\right)\\&\quad+\frac{r_3}{\mu_1}\boldsymbol{y}_D^{\mathrm{T}}\left[\frac{r_1\left(\mu_1-\mu_2\right)}{\mu_2}\boldsymbol{P}_3-\frac{r_2\left(\mu_1^2-\mu_2^2\right)}{\mu_2^2}\boldsymbol{P}_2\right]\mathrm{sat}\left(\frac{\boldsymbol{y}_{\mu_1}}{r_3}\right)\\&\quad+\frac{\lambda}{\mu_1}\left[\boldsymbol{y}_D^{\mathrm{T}}-r_1\boldsymbol{y}_{\mu_1}^{\mathrm{T}}-\frac{r_1r_3\left(\mu_1-\mu_2\right)}{\mu_2}\mathrm{sat}^{\mathrm{T}}\left(\frac{\boldsymbol{y}_{\mu_1}}{r_3}\right)\right]\mathrm{sat}\left(\frac{\boldsymbol{y}_{\mu_1}}{r_3}\right)\\&\quad+\left(\boldsymbol{y}_D^{\mathrm{T}}\boldsymbol{P}_2-\boldsymbol{y}_{\mu_1}^{\mathrm{T}}\boldsymbol{P}_3\right)\dot{\boldsymbol{D}}.\end{aligned}\tag{13}$$

Let matrices $\boldsymbol{P}_i$, $(i = 1, 2, 3)$ and the constant λ satisfies the following conditions

$$\begin{cases}\boldsymbol{P}_1-\boldsymbol{P}_3>0,\\ \boldsymbol{P}_2-\boldsymbol{P}_3>0,\\ r_1\boldsymbol{P}_1-r_2\boldsymbol{P}_3>0,\\ \boldsymbol{P}_1-r_2\boldsymbol{P}_2+r_1\boldsymbol{P}_3=\boldsymbol{0},\\ r_2r_3\left(\mu_1^2/\mu_2^2-1\right)\boldsymbol{P}_2-r_1r_3\left(\mu_1/\mu_2-1\right)\boldsymbol{P}_3=\lambda\boldsymbol{I}.\end{cases}\tag{14}$$

Then, it can be deduced that

$$\begin{aligned}&\dot{V}_1\\&=-\frac{\boldsymbol{y}_{\mu_1}^{\mathrm{T}}\left(r_1\boldsymbol{P}_1-r_2\boldsymbol{P}_3\right)\boldsymbol{y}_{\mu_1}}{\mu_1}-\frac{\boldsymbol{y}_D^{\mathrm{T}}\boldsymbol{P}_3\boldsymbol{y}_D}{\mu_1}+\left(\boldsymbol{y}_D^{\mathrm{T}}\boldsymbol{P}_2-\boldsymbol{y}_{\mu_1}^{\mathrm{T}}\boldsymbol{P}_3\right)\dot{\boldsymbol{D}}\\&\quad+\frac{\boldsymbol{y}_{\mu_1}^{\mathrm{T}}}{\mu_1}\left[-r_1\lambda\boldsymbol{I}+\frac{r_2r_3\left(\mu_1^2-\mu_2^2\right)}{\mu_2^2}\boldsymbol{P}_3\right.\\&\quad\left.-\frac{r_1r_3\left(\mu_1-\mu_2\right)}{\mu_2}\boldsymbol{P}_1\right]\mathrm{sat}\left(\frac{\boldsymbol{y}_{\mu_1}}{r_3}\right)\\&\quad-\frac{r_1r_3\lambda\left(\mu_1-\mu_2\right)}{\mu_1\mu_2}\mathrm{sat}^{\mathrm{T}}\left(\frac{\boldsymbol{y}_{\mu_1}}{r_3}\right)\mathrm{sat}\left(\frac{\boldsymbol{y}_{\mu_1}}{r_3}\right).\end{aligned}\tag{15}$$

According to the previous constraint $\mu_2 < \mu_1$ and condition (14), we have

$$-r_1\lambda\boldsymbol{I}+\frac{r_2r_3\boldsymbol{P}_3\left(\mu_1^2-\mu_2^2\right)}{\mu_2^2}-\frac{r_1r_3\boldsymbol{P}_1\left(\mu_1-\mu_2\right)}{\mu_2}<0\tag{16}$$

To describe the subsequent proof clearly, the following two compact sets are introduced

$$\begin{aligned}\Pi_1&=\left\{\boldsymbol{y}\in\mathbb{R}^6|V_1(\boldsymbol{y})\leq K_1\right\}\\ \Pi_2&=\left\{\boldsymbol{y}\in\mathbb{R}^6|V_1(\boldsymbol{y})\leq K_2\right\}\end{aligned}\tag{17}$$

where Π_2 is a positive constant such that $\max_{\boldsymbol{y}\in\Pi_2}\{y_{\mu_1}^1, y_{\mu_1}^2, y_{\mu_1}^3\}\leq r_3$ and $\Pi_1 = \max\{V_1(0), \Pi_2\}$. Then, the following two steps would be given to complete the subsequent proof.

Step 1: Consider the situation that if $\boldsymbol{y}\in\Pi_1-\Pi_2$, there exists a moment t_{μ_1} such that $\boldsymbol{y}\in\Pi_2$ for $\forall t\geq t_{\mu_1}$. On account of the different value of the $\left(\boldsymbol{y}_{\mu_1}/r_3\right)$, the following two cases would be discussed, respectively.

Case A: For $\left|y_{\mu_1}^i\right|\leq r_3$, $i = 1, 2, 3$, we have

$$\begin{aligned}\mathrm{sat}\left(\frac{\boldsymbol{y}_{\mu_1}}{r_3}\right)&=\left[\mathrm{sat}\left(\frac{y_{\mu_1}^1}{r_3}\right),\mathrm{sat}\left(\frac{y_{\mu_1}^2}{r_3}\right),\mathrm{sat}\left(\frac{y_{\mu_1}^3}{r_3}\right)\right]^{\mathrm{T}}\\&=\left[\frac{y_{\mu_1}^1}{r_3},\frac{y_{\mu_1}^2}{r_3},\frac{y_{\mu_1}^3}{r_3}\right]^{\mathrm{T}}=\frac{\boldsymbol{y}_{\mu_1}}{r_3}.\end{aligned}\tag{18}$$

Thus, combing with the Young's inequality [38], the Lyapunov function (11) can be rewritten as follows

$$\begin{aligned}V_1&=\frac{1}{2}\left(\boldsymbol{y}_{\mu_1}^{\mathrm{T}}\boldsymbol{P}_1\boldsymbol{y}_{\mu_1}+\boldsymbol{y}_D^{\mathrm{T}}\boldsymbol{P}_2\boldsymbol{y}_D-2\boldsymbol{y}_{\mu_1}^{\mathrm{T}}\boldsymbol{P}_3\boldsymbol{y}_D\right)+\frac{\lambda}{2r_3}\boldsymbol{y}_{\mu_1}^{\mathrm{T}}\boldsymbol{y}_{\mu_1}\\&\leq\frac{1}{2}\left\|\boldsymbol{P}_1+\boldsymbol{P}_3+\frac{\lambda}{r_3}\boldsymbol{I}\right\|\left\|\boldsymbol{y}_{\mu_1}\right\|^2+\frac{1}{2}\left\|\boldsymbol{P}_2+\boldsymbol{P}_3\right\|\left\|\boldsymbol{y}_D\right\|^2,\end{aligned}\tag{19}$$

According to the Assumption 1 and conditions (14), we can be obtained that

$$\begin{aligned}\dot{V}_1 &= -\frac{\boldsymbol{y}_{\mu_1}^{\mathrm{T}}\left(r_1\boldsymbol{P}_1-r_2\boldsymbol{P}_3\right)\boldsymbol{y}_{\mu_1}}{\mu_1}-\frac{\boldsymbol{y}_D^{\mathrm{T}}\boldsymbol{P}_3\boldsymbol{y}_D}{\mu_1}+\left(\boldsymbol{y}_D^{\mathrm{T}}\boldsymbol{P}_2-\boldsymbol{y}_{\mu_1}^{\mathrm{T}}\boldsymbol{P}_3\right)\dot{\boldsymbol{D}}\\ &\quad+\frac{\boldsymbol{y}_{\mu_1}^{\mathrm{T}}}{\mu_1}\left[-\frac{r_1\lambda}{r_3}\boldsymbol{I}+\frac{r_2\left(\mu_1^2-\mu_2^2\right)}{\mu_2^2}\boldsymbol{P}_3-\frac{r_1\left(\mu_1-\mu_2\right)}{\mu_2}\boldsymbol{P}_1\right]\boldsymbol{y}_{\mu_1}\\ &\quad-\frac{r_1\lambda\left(\mu_1-\mu_2\right)}{\mu_1\mu_2 r_3}\boldsymbol{y}_{\mu_1}^{\mathrm{T}}\boldsymbol{y}_{\mu_1}\\ &=-\frac{1}{\mu_1}\boldsymbol{y}_{\mu_1}^{\mathrm{T}}\left(\frac{r_1\lambda}{r_3}\frac{\mu_1}{\mu_2}\boldsymbol{I}+r_1\frac{\mu_1}{\mu_2}\boldsymbol{P}_1-r_2\frac{\mu_1^2}{\mu_2^2}\boldsymbol{P}_3\right)\boldsymbol{y}_{\mu_1}-\frac{\boldsymbol{y}_D^{\mathrm{T}}\boldsymbol{P}_3\boldsymbol{y}_D}{\mu_1}\\ &\quad+\left(\boldsymbol{y}_D^{\mathrm{T}}\boldsymbol{P}_2-\boldsymbol{y}_{\mu_1}^{\mathrm{T}}\boldsymbol{P}_3\right)\dot{\boldsymbol{D}}\\ &\le-\frac{1}{2\mu_1}\left(\boldsymbol{y}_{\mu_1}^{\mathrm{T}}\boldsymbol{\Gamma}_1\boldsymbol{y}_{\mu_1}+\boldsymbol{y}_D^{\mathrm{T}}\boldsymbol{P}_3\boldsymbol{y}_D\right)+g_1d_2\left\|\boldsymbol{y}\right\|-\frac{1}{2\mu_1}g_2\left\|\boldsymbol{y}\right\|^2,\end{aligned}\tag{20}$$

where $\boldsymbol{\Gamma}_1 \triangleq \frac{r_1\lambda}{r_3}\frac{\mu_1}{\mu_2}\boldsymbol{I}+r_1\frac{\mu_1}{\mu_2}\boldsymbol{P}_1-r_2\frac{\mu_1^2}{\mu_2^2}\boldsymbol{P}_3$, $g_1=\|\boldsymbol{P}_2\|+\|\boldsymbol{P}_3\|$, and g_2 denotes the minimum eigenvalue of the matrix $\mathrm{diag}\{\boldsymbol{\Gamma}_1,\boldsymbol{P}_3\}$.

Let $\mu_1 \le \frac{g_2}{2g_1d_2}\min\limits_{\boldsymbol{y}\in\Pi_1-\Pi_2}\|\boldsymbol{y}\|$, it yields

$$\begin{aligned}\dot{V}_1 &\le -\frac{1}{2\mu_1}\left(\boldsymbol{y}_{\mu_1}^{\mathrm{T}}\boldsymbol{\Gamma}_1\boldsymbol{y}_{\mu_1}+\boldsymbol{y}_D^{\mathrm{T}}\boldsymbol{P}_3\boldsymbol{y}_D\right)-\|\boldsymbol{y}\|\left(\frac{g_2}{2\mu_1}\|\boldsymbol{y}\|-g_1d_2\right)\\ &\le -\frac{1}{2\mu_1}\left(\boldsymbol{y}_{\mu_1}^{\mathrm{T}}\boldsymbol{\Gamma}_1\boldsymbol{y}_{\mu_1}+\boldsymbol{y}_D^{\mathrm{T}}\boldsymbol{P}_3\boldsymbol{y}_D\right)\le\frac{g_3}{\mu_1}V_1\end{aligned}\tag{21}$$

where $g_3=\min\left\{\frac{\lambda_{\min}(\boldsymbol{\Gamma}_1)}{\|\boldsymbol{P}_1+\boldsymbol{P}_3+\lambda/r_3\boldsymbol{I}\|},\frac{\lambda_{\min}(\boldsymbol{P}_3)}{\|\boldsymbol{P}_2+\boldsymbol{P}_3\|}\right\}$.

Case B: For $\forall\left|y_{\mu_1}^i\right|>r_3$, $i=1,2,3$, we have

$$\mathrm{sat}\left(\frac{\boldsymbol{y}_{\mu_1}}{r_3}\right)=\mathrm{sgn}\left(\boldsymbol{y}_{\mu_1}\right)\tag{22}$$

In order to avoid the awkward phrasing, define the n as the number of $y_{\mu_1}^i$ such that $\left|y_{\mu_1}^i\right|>r_3$, and m denotes the number of $y_{\mu_1}^i$ such that $\left|y_{\mu_1}^i\right|\le r_3$. Then, substituting (22) into (11) yields

$$\begin{aligned}V_1&=\frac{1}{2}\left(\boldsymbol{y}_{\mu_1}^{\mathrm{T}}\boldsymbol{P}_1\boldsymbol{y}_{\mu_1}+\boldsymbol{y}_D^{\mathrm{T}}\boldsymbol{P}_2\boldsymbol{y}_D-2\boldsymbol{y}_{\mu_1}^{\mathrm{T}}\boldsymbol{P}_3\boldsymbol{y}_D\right)+\sum_{i=1}^{m}\frac{\lambda}{2r_3}\left(y_{\mu_1}^i\right)^2\\ &\quad+\sum_{j=1}^{n}\left(\lambda\left|y_{\mu_1}^j\right|-\frac{\lambda r_3}{2}\right)\\ &\le\frac{1}{2}\boldsymbol{y}_{\mu_1}^{\mathrm{T}}\left(\boldsymbol{P}_1+\boldsymbol{P}_3+\frac{\lambda}{r_3}\boldsymbol{I}\right)\boldsymbol{y}_{\mu_1}+\frac{1}{2}\boldsymbol{y}_D^{\mathrm{T}}\left(\boldsymbol{P}_2+\boldsymbol{P}_3\right)\boldsymbol{y}_D\\ &\quad+\sum_{j=1}^{n}\left(\lambda\left|y_{\mu_1}^j\right|-\frac{\lambda r_3}{2}\right)\\ &\le\frac{1}{2}\left\|\boldsymbol{P}_1+\boldsymbol{P}_3+\frac{\lambda}{r_3}\boldsymbol{I}\right\|\left\|\boldsymbol{y}_{\mu_1}\right\|^2+\frac{1}{2}\left\|\boldsymbol{P}_2+\boldsymbol{P}_3\right\|\left\|\boldsymbol{y}_D\right\|^2\\ &\quad+\sum_{j=1}^{n}\left(\lambda\left|y_{\mu_1}^j\right|-\frac{\lambda r_3}{2}\right)\end{aligned}\tag{23}$$

Combined with the (15) and the Young's inequality [38], we have

$$\begin{aligned}\dot{V}_1 &\le -\frac{\boldsymbol{y}_{\mu_1}^{\mathrm{T}}\left(r_1\boldsymbol{P}_1-r_2\boldsymbol{P}_3\right)\boldsymbol{y}_{\mu_1}}{\mu_1}-\frac{\boldsymbol{y}_D^{\mathrm{T}}\boldsymbol{P}_3\boldsymbol{y}_D}{\mu_1}\\ &\quad+g_1d_2\left\|\boldsymbol{y}\right\|-\frac{1}{\mu_1}\sum_{i=1}^{n}\left|y_{\mu_1}^i\right|\Gamma_2^i\\ &\quad-\sum_{j=1}^{n}\left(\frac{r_1r_3\lambda(\mu_1\mu_2-\mu_2)}{\mu_1\mu_2}\right)\\ &\le-\frac{1}{2\mu_1}\boldsymbol{y}_{\mu_1}^{\mathrm{T}}\left(r_1\boldsymbol{P}_1-r_2\boldsymbol{P}_3\right)\boldsymbol{y}_{\mu_1}-\frac{1}{2\mu_1}\boldsymbol{y}_D^{\mathrm{T}}\boldsymbol{P}_3\boldsymbol{y}_D+g_1d_2\left\|\boldsymbol{y}\right\|\\ &\quad-\frac{1}{2\mu_1}g_4\left\|\boldsymbol{y}\right\|^2-\frac{g_5}{\mu_1}\sum_{j=1}^{n}\left(\left|y_{\mu_1}^i\right|-\frac{r_3}{2}\right)\end{aligned}\tag{24}$$

where $\boldsymbol{\Gamma}_2=r_1\lambda\boldsymbol{I}+\frac{r_1r_3(\mu_1-\mu_2)}{\mu_2}\boldsymbol{P}_1-\frac{r_2r_3\left(\mu_1^2-\mu_2^2\right)}{\mu_2^2}\boldsymbol{P}_3$ is a positive definite symmetric matrix, Γ_2^i denotes the i-th diagonal element for $\boldsymbol{\Gamma}_2$, g_4 is the minimum eigenvalue of the matrix $diag\left\{\left(r_1\boldsymbol{P}_1-r_2\boldsymbol{P}_3\right),\boldsymbol{P}_3\right\}$, g_5 is the minimum eigenvalue of the matrix $\boldsymbol{\Gamma}_2$.

Let $\mu_1 \le \frac{g_4}{2g_1d_2}\min\limits_{\boldsymbol{y}\in\Pi_1-\Pi_2}\|\boldsymbol{y}\|$, equation (24) can be expressed as

$$\begin{aligned}\dot{V}_1 &\le -\frac{1}{2\mu_1}\boldsymbol{y}_{\mu_1}^{\mathrm{T}}\left(r_1\boldsymbol{P}_1-r_2\boldsymbol{P}_3\right)\boldsymbol{y}_{\mu_1}\\ &\quad-\frac{1}{2\mu_1}\boldsymbol{y}_D^{\mathrm{T}}\boldsymbol{P}_3\boldsymbol{y}_D-\frac{g_5}{\mu_1}\sum_{j=1}^{n}\left(\left|y_{\mu_1}^i\right|-\frac{r_3}{2}\right)\\ &\le-\frac{g_6}{\mu_1}V_1\end{aligned}\tag{25}$$

where $g_6=\min\left\{\frac{\lambda_{\min}(r_1\boldsymbol{P}_1-r_2\boldsymbol{P}_3)}{\|\boldsymbol{P}_1+\boldsymbol{P}_3+\lambda/r_3\boldsymbol{I}\|},\frac{\lambda_{\min}(\boldsymbol{P}_3)}{\|\boldsymbol{P}_2+\boldsymbol{P}_3\|},\frac{\min(\boldsymbol{\Gamma}_2)}{\lambda}\right\}$.

According to the (21) and (25), utilizing the comparison principle of ordinary differential equations, one can further obtain that

$$V_1\left(\boldsymbol{y}(t)\right)\le e^{-\frac{g_7}{\upsilon_1}}V_1\left(\boldsymbol{y}(0)\right)\tag{26}$$

where $\upsilon_1 \le \min\left\{\frac{g_2}{2g_1d_2}\min\limits_{\boldsymbol{y}\in\Pi_1-\Pi_2}\|\boldsymbol{y}\|,\frac{g_4}{2g_1d_2}\min\limits_{\boldsymbol{y}\in\Pi_1-\Pi_2}\|\boldsymbol{y}\|\right\}$ and $g_7=\min\{g_3,g_6\}$.

Therefore, it can be obtained that $\boldsymbol{y}\in\Pi_2$, for $\forall t\ge t_{\mu_1}=\frac{\upsilon_1}{g_7}\ln\left(\frac{K_1}{K_2}\right)$, which means that even $\boldsymbol{y}\in\Pi_1-\Pi_2$, the $V(\boldsymbol{y})$ would decrease until $\boldsymbol{y}\in\Pi_2$ again.

Step 2: Consider the situation that $\boldsymbol{y}\in\Pi_2$, we have $\left|y_{\mu_1}^i\right|\le r_3$, $(i=1,2,3)$, for $\forall t\ge t_{\mu_1}$. Thus, the following estimation error system can be obtained

$$\begin{cases}\dot{\boldsymbol{y}}_{\mu_2}=\dfrac{\boldsymbol{y}_D-r_1\boldsymbol{y}_{\mu_2}}{\mu_2}\\ \dot{\boldsymbol{y}}_D=-\dfrac{r_2}{\mu_2}\boldsymbol{y}_{\mu_2}+\dot{\boldsymbol{D}}\end{cases}\tag{27}$$

Select the Lyapunov function candidate as follows

$$V_2=\frac{1}{2}\left(\boldsymbol{y}_{\mu_2}^{\mathrm{T}}\boldsymbol{P}_1\boldsymbol{y}_{\mu_2}+\boldsymbol{y}_D^{\mathrm{T}}\boldsymbol{P}_2\boldsymbol{y}_D-2\boldsymbol{y}_{\mu_2}^{\mathrm{T}}\boldsymbol{P}_3\boldsymbol{y}_D\right)\tag{28}$$

Based on the Young's inequality [38], we have

$$\frac{1}{2}\boldsymbol{y}_{\mu_2}^{\mathrm{T}}(\boldsymbol{P}_1-\boldsymbol{P}_3)\boldsymbol{y}_{\mu_2}+\frac{1}{2}\boldsymbol{y}_D^{\mathrm{T}}(\boldsymbol{P}_2-\boldsymbol{P}_3)\boldsymbol{y}_D \le V_2 \le \frac{1}{2}\boldsymbol{y}_{\mu_2}^{\mathrm{T}}(\boldsymbol{P}_1+\boldsymbol{P}_3)\boldsymbol{y}_{\mu_2}+\frac{1}{2}\boldsymbol{y}_D^{\mathrm{T}}(\boldsymbol{P}_2+\boldsymbol{P}_3)\boldsymbol{y}_D \tag{29}$$

So, the time derivative of V_2 can be obtained

$$\begin{aligned}\dot{V}_2&=\left(\boldsymbol{y}_{\mu_2}^{\mathrm{T}}\boldsymbol{P}_1-\boldsymbol{y}_D^{\mathrm{T}}\boldsymbol{P}_3\right)\dot{\boldsymbol{y}}_{\mu_2}+\left(\boldsymbol{y}_D^{\mathrm{T}}\boldsymbol{P}_2-\boldsymbol{y}_{\mu_2}^{\mathrm{T}}\boldsymbol{P}_3\right)\dot{\boldsymbol{y}}_D\\&=-\frac{\boldsymbol{y}_{\mu_2}^{\mathrm{T}}(r_1\boldsymbol{P}_1-r_2\boldsymbol{P}_3)\boldsymbol{y}_{\mu_2}}{\mu_2}-\frac{\boldsymbol{y}_D^{\mathrm{T}}\boldsymbol{P}_3\boldsymbol{y}_D}{\mu_2}+\left(\boldsymbol{y}_D^{\mathrm{T}}\boldsymbol{P}_2-\boldsymbol{y}_{\mu_2}^{\mathrm{T}}\boldsymbol{P}_3\right)\dot{\boldsymbol{D}}\end{aligned} \tag{30}$$

Then, it yields

$$\begin{aligned}\dot{V}_2&\le-\frac{\boldsymbol{y}_{\mu_2}^{\mathrm{T}}(r_1\boldsymbol{P}_1-r_2\boldsymbol{P}_3)\boldsymbol{y}_{\mu_2}}{\mu_2}-\frac{\boldsymbol{y}_D^{\mathrm{T}}\boldsymbol{P}_3\boldsymbol{y}_D}{\mu_2}+g_1d_2\|\bar{\boldsymbol{y}}\|\\&\le-\frac{g_8}{\mu_2}V_2+g_1d_2\sqrt{\frac{V_2}{g_9}}\end{aligned} \tag{31}$$

where $g_8=\min\left\{\frac{2\lambda_{\min}(r_1\boldsymbol{P}_1-r_2\boldsymbol{P}_3)}{\|\boldsymbol{P}_1+\boldsymbol{P}_3\|},\frac{2\lambda_{\min}(\boldsymbol{P}_3)}{\|\boldsymbol{P}_2+\boldsymbol{P}_3\|}\right\}$ and g_9 denotes the minimum eigenvalue of the matrix $\mathrm{diag}\left\{\frac{\boldsymbol{P}_1-\boldsymbol{P}_3}{2},\frac{\boldsymbol{P}_2-\boldsymbol{P}_3}{2}\right\}$.

On account of the Eq. (31), it can be found that if $V_2>\frac{4g_1^2\mu_2^2d_2^2}{g_8^2g_9}$, we have

$$\dot{V}_2\le-\frac{g_8}{\mu_2}V_2+g_1d_2\sqrt{\frac{V_2}{g_9}}\le-\frac{g_8}{2\mu_2}V_2<0 \tag{32}$$

According to the comparison principle of ordinary differential equations, it follows that

$$V_2(\bar{\boldsymbol{y}}(t))\le e^{-\frac{g_8}{2\mu_2}(t-t_{\mu_1})}V_2\left(\bar{\boldsymbol{y}}\left(t_{\mu_1}\right)\right) \tag{33}$$

Recalling the definition $\boldsymbol{y}$ and $\bar{\boldsymbol{y}}$, we can conclude that when $t\ge t_{\mu_1}, \boldsymbol{y}\in\Pi_2$, and there exists a positive constant K_3 such that $V_2(\bar{\boldsymbol{y}}(t))\le K_3$. Then, for $t\ge t_{\mu_1}+t_{\mu_2}$, where $t_{\mu_2}\triangleq\frac{2\mu_2}{g_8}\ln\left(\frac{\max\{4g_1^2\mu_2^2d_2^2/g_8^2g_9,K_3\}}{4g_1^2\mu_2^2d_2^2/g_8^2g_9}\right)$, we can obtain that

$$V_2\le\frac{4g_1^2\mu_2^2d_2^2}{g_8^2g_9} \tag{34}$$

Besides, on basis of the (28), it holds that

$$\|\bar{\boldsymbol{y}}(t)\|\le\sqrt{\frac{V_2(\bar{\boldsymbol{y}}(t))}{g_9}}\le\frac{2g_1\mu_2^2d_2}{g_8g_9} \tag{35}$$

$$\|\boldsymbol{e}_2(t)-\tilde{\boldsymbol{e}}_2(t)\|=\mu_2\left\|\boldsymbol{y}_{\mu_2}(t)\right\|\le\mu_2\|\bar{\boldsymbol{y}}(t)\|\le\frac{2g_1\mu_2^2d_2}{g_8g_9} \tag{36}$$

$$\left\|\boldsymbol{D}(t)-\tilde{\boldsymbol{D}}(t)\right\|=\left\|\boldsymbol{y}_D(t)\right\|\le\|\bar{\boldsymbol{y}}(t)\|\le\frac{2g_1\mu_2d_2}{g_8g_9} \tag{37}$$

Therefore, it can be concluded that the estimation errors $\|\boldsymbol{e}_2-\tilde{\boldsymbol{e}}_2\|$ and $\left\|\boldsymbol{D}-\tilde{\boldsymbol{D}}\right\|$ would converge to some small residual set of zero for $t>t_{\mu_1}+t_{\mu_2}$. ■

Remark 2: It can be seen form the proposed ESO (9) that there are two different form of the observer caused by the saturation function $\mathrm{sat}\left(\frac{1}{\mu_1r_3}(\boldsymbol{e}_2-\tilde{\boldsymbol{e}}_2)\right)$. For $\left|\frac{e_2^i-\tilde{e}_2^i}{\mu_1r_3}\right|\le1, i=1,2,3$, the corresponding observer is given as follows

$$\begin{cases}\dot{\tilde{\boldsymbol{e}}}_2=\boldsymbol{F}\boldsymbol{\omega}+\boldsymbol{G}_1\boldsymbol{\delta}+\tilde{\boldsymbol{D}}+\dfrac{r_1}{\mu_2}(\boldsymbol{e}_2-\tilde{\boldsymbol{e}}_2)\\ \dot{\tilde{\boldsymbol{D}}}=\dfrac{r_2}{\mu_2^2}(\boldsymbol{e}_2-\tilde{\boldsymbol{e}}_2)\end{cases} \tag{38}$$

Thus, it is obvious that the observer operates within a larger linear region attributed to the parameter μ_2 during the steady phase. Conversely, when $\left|\frac{e_2^i-\tilde{e}_2^i}{\mu_1r_3}\right|>1, i=1,2,3$, the following form of the observer can be obtained

$$\begin{cases}\dot{\tilde{\boldsymbol{e}}}_2=\boldsymbol{F}\boldsymbol{\omega}+\boldsymbol{G}_1\boldsymbol{\delta}+\tilde{\boldsymbol{D}}+r_1\left[\dfrac{\boldsymbol{e}_2-\tilde{\boldsymbol{e}}_2}{\mu_1}+\dfrac{r_3(\mu_1-\mu_2)}{\mu_2}\mathrm{sgn}(\boldsymbol{e}_2-\tilde{\boldsymbol{e}}_2)\right]\\ \dot{\tilde{\boldsymbol{D}}}=r_2\left[\dfrac{1}{\mu_1^2}(\boldsymbol{e}_2-\tilde{\boldsymbol{e}}_2)+\dfrac{r_3(\mu_1^2-\mu_2^2)}{\mu_1\mu_2^2}\mathrm{sgn}(\boldsymbol{e}_2-\tilde{\boldsymbol{e}}_2)\right]\end{cases} \tag{39}$$

It can be found that the observer operates within a smaller linear region due to the parameter μ_2 during the transient phase. Similarly, a sliding mode-like term is employed to improve the performances of the observer [35].

B. FAULT TOLERANT CONTROL SCHEME DESIGN

Utilizing the proposed ESO (9), we have obtained the estimation vector $\tilde{\boldsymbol{D}}$ for compound disturbances, including external disturbances and fault informations. Next, the main aim is to design a fault tolerant controller to maintain the system tracking performance.

For system (8) with actuator faults, the following integral terminal sliding mode surface is designed

$$\boldsymbol{s}=\boldsymbol{e}_2+\int_0^t\left(l_1\boldsymbol{e}_1\|\boldsymbol{e}_1\|^{a-1}+l_2\boldsymbol{e}_2\|\boldsymbol{e}_2\|^{b-1}\right)dt \tag{40}$$

where l_1 and l_2 are positive constants, $0<b<1$ and $a=\frac{2b}{2-b}$. With the help of the proposed ESO (9), the sliding mode fault tolerant control law is proposed as follows

$$\boldsymbol{\delta}=-\boldsymbol{G}_1^{-1}\left(\boldsymbol{F}\boldsymbol{\omega}+\tilde{\boldsymbol{D}}-\ddot{\boldsymbol{\xi}}_c+l_1\boldsymbol{e}_1\|\boldsymbol{e}_1\|^{a-1}+l_2\boldsymbol{e}_2\|\boldsymbol{e}_2\|^{b-1}+\zeta_1\boldsymbol{s}+\zeta_2\boldsymbol{s}\|\boldsymbol{s}\|^{c-1}\right) \tag{41}$$

where the ζ_i, $(i=1,2)$ and c are controller parameters, which would be determined later.

Theorem 2: Consider the attitude tracking error systems (8) subject to actuator faults (5), if the fault tolerant control law designed as the (34), the control parameters $\zeta_i>0, (i=1,2)$ and $0<c<1$, then the stability of the closed-loop system would be guaranteed even existing the system uncertainties and actuator malfunctions.

Proof: The derivative of sliding mode surface (33) with respect to time yields that

$$\dot{\boldsymbol{s}}=\dot{\boldsymbol{e}}_2+l_1\boldsymbol{e}_1\|\boldsymbol{e}_1\|^{a-1}+l_2\boldsymbol{e}_2\|\boldsymbol{e}_2\|^{b-1} \tag{42}$$

According to the (8) and (34), it follows that

$$\begin{aligned}\dot{\boldsymbol{s}} &= \boldsymbol{F}\boldsymbol{\omega} + \boldsymbol{G}_1\boldsymbol{\delta} + \boldsymbol{D} - \ddot{\boldsymbol{\xi}}_c + l_1\boldsymbol{e}_1\left\|\boldsymbol{e}_1\right\|^{a-1} + l_2\boldsymbol{e}_2\left\|\boldsymbol{e}_2\right\|^{b-1} \\ &= \boldsymbol{D} - \tilde{\boldsymbol{D}} - \zeta_1\boldsymbol{s} - \zeta_2\boldsymbol{s}\left\|\boldsymbol{s}\right\|^{c-1} \\ &= \boldsymbol{y}_D - \zeta_1\boldsymbol{s} - \zeta_2\boldsymbol{s}\left\|\boldsymbol{s}\right\|^{c-1} \end{aligned} \tag{43}$$

Choose the Lyapunov function candidate as

$$W_1 = \frac{1}{2}\boldsymbol{s}^{\mathrm{T}}\boldsymbol{s} + \frac{1}{2}\boldsymbol{e}_1^{\mathrm{T}}\boldsymbol{e}_1 + \frac{1}{2}\boldsymbol{e}_2^{\mathrm{T}}\boldsymbol{e}_2 \tag{44}$$

Besides, we can conclude that $\|\boldsymbol{e}_1\|^a \le 1 + \|\boldsymbol{e}_1\|$ for $0 < a < 1$. Similarly, the inequalities $\|\boldsymbol{e}_2\|^b \le 1 + \|\boldsymbol{e}_2\|$ and $\|\boldsymbol{s}\|^c \le 1 + \|\boldsymbol{s}\|$ are true. Thus, the derivative of W_1 along the trajectories of (8) can be obtained as follows

$$\begin{aligned}\dot{W}_1 &= \boldsymbol{s}^{\mathrm{T}}\dot{\boldsymbol{s}} + \boldsymbol{e}_1^{\mathrm{T}}\dot{\boldsymbol{e}}_1 + \boldsymbol{e}_2^{\mathrm{T}}\dot{\boldsymbol{e}}_2 \\ &= \boldsymbol{s}^{\mathrm{T}}\dot{\boldsymbol{s}} + \boldsymbol{e}_1^{\mathrm{T}}\boldsymbol{e}_2 + \boldsymbol{e}_2^{\mathrm{T}}\left(\dot{\boldsymbol{s}} - l_1\left\|\boldsymbol{e}_1\right\|^a\frac{\boldsymbol{e}_1}{\|\boldsymbol{e}_1\|} - l_2\left\|\boldsymbol{e}_2\right\|^b\frac{\boldsymbol{e}_2}{\|\boldsymbol{e}_2\|}\right) \\ &\le \left\|\boldsymbol{s}^{\mathrm{T}}\boldsymbol{y}_D\right\| + \left\|\boldsymbol{e}_1^{\mathrm{T}}\boldsymbol{e}_2\right\| + \|\boldsymbol{e}_2\|\left\|\boldsymbol{y}_D\right\| \\ &\quad + \zeta_1\|\boldsymbol{e}_2\|\|\boldsymbol{s}\| + \zeta_2\|\boldsymbol{e}_2\|(1+\|\boldsymbol{s}\|) \\ &\quad + l_1\|\boldsymbol{e}_2\|(1+\|\boldsymbol{e}_1\|) + l_2\|\boldsymbol{e}_2\|(1+\|\boldsymbol{e}_2\|) \\ &\le \frac{1}{2}\left(\|\boldsymbol{s}\|^2 + \left\|\boldsymbol{y}_D\right\|^2\right) + \frac{1}{2}\left(\|\boldsymbol{e}_1\|^2 + \|\boldsymbol{e}_2\|^2\right) \\ &\quad + \frac{1}{2}\left(\|\boldsymbol{e}_2\|^2 + \left\|\boldsymbol{y}_D\right\|^2\right) \\ &\quad + \frac{1}{2}(\zeta_1+\zeta_2)\left(\|\boldsymbol{e}_2\|^2 + \|\boldsymbol{s}\|^2\right) \\ &\quad + \frac{1}{2}\left(\zeta_2^2 + \|\boldsymbol{s}\|^2\right) + \frac{1}{2}\left(l_1^2 + \|\boldsymbol{e}_2\|^2\right) \\ &\quad + \frac{l_1}{2}\left(\|\boldsymbol{e}_1\|^2 + \|\boldsymbol{e}_2\|^2\right) \\ &\quad + \frac{1}{2}\left(l_2^2 + \|\boldsymbol{e}_2\|^2\right) + l_2\|\boldsymbol{e}_2\|^2 \\ &= \frac{1+\zeta_1+\zeta_2}{2}\|\boldsymbol{s}\|^2 + \frac{1+l_1}{2}\|\boldsymbol{e}_1\|^2 \\ &\quad + \frac{4+\zeta_1+\zeta_2+l_1+2l_2}{2}\|\boldsymbol{e}_2\|^2 \\ &\quad + \left\|\boldsymbol{y}_D\right\|^2 + \frac{\zeta_2^2}{2} + \frac{l_1^2+l_2^2}{2} \\ &\le rW_1 + l \end{aligned} \tag{45}$$

where $r \triangleq 4 + \zeta_1 + \zeta_2 + l_1 + 2l_2$ and $l \triangleq \max\left\{\left\|\boldsymbol{y}_D\right\|^2 + \zeta_2^2/2\ \left(l_1^2 + l_2^2\right)/2\right\}$. According to the Theorem 1, the estimation error $\boldsymbol{y}_D$ would converge to some small residual set of zero, i.e., the l is bounded. Thus, the derivative of sliding mode $\boldsymbol{s}$ can be rewritten as

$$\dot{\boldsymbol{s}} = -\zeta_1\boldsymbol{s} - \zeta_2\boldsymbol{s}\left\|\boldsymbol{s}\right\|^{c-1} \tag{46}$$

It is obvious that (38) is finite time stable. Once the sliding mode surface is reached, i.e., $\dot{\boldsymbol{s}} = 0$, we have

$$\dot{\boldsymbol{e}}_2 + l_1\boldsymbol{e}_1\left\|\boldsymbol{e}_1\right\|^{a-1} + l_2\boldsymbol{e}_2\left\|\boldsymbol{e}_2\right\|^{b-1} = 0 \tag{47}$$

Then, (8) can be converted to

$$\begin{cases}\dot{\boldsymbol{e}}_1 = \boldsymbol{e}_2 \\ \dot{\boldsymbol{e}}_2 = -l_1\boldsymbol{e}_1\left\|\boldsymbol{e}_1\right\|^{a-1} - l_2\boldsymbol{e}_2\left\|\boldsymbol{e}_2\right\|^{b-1}\end{cases} \tag{48}$$

Selecting the Lyapunov function as

$$W_2 = l_1\frac{\left\|\boldsymbol{e}_1\right\|^{a+1}}{a+1} + \frac{1}{2}\left\|\boldsymbol{e}_2\right\|^2 \tag{49}$$

The derivative of W_2 is given as follows

$$\begin{aligned}\dot{W}_2 &= l_1\left\|\boldsymbol{e}_1\right\|^{a-1}\boldsymbol{e}_1^{\mathrm{T}}\dot{\boldsymbol{e}}_1 + \boldsymbol{e}_2^{\mathrm{T}}\dot{\boldsymbol{e}}_2 \\ &= l_1\left\|\boldsymbol{e}_1\right\|^{a-1}\boldsymbol{e}_1^{\mathrm{T}}\boldsymbol{e}_2 - \boldsymbol{e}_2^{\mathrm{T}}\left(l_1\boldsymbol{e}_1\left\|\boldsymbol{e}_1\right\|^{a-1} + l_2\boldsymbol{e}_2\left\|\boldsymbol{e}_2\right\|^{b-1}\right) \\ &= -l_2\left\|\boldsymbol{e}_2\right\|^{b+1} \le 0 \end{aligned} \tag{50}$$

Therefore, the system (8) is asymptotic stable. In addition, for the vector space (48), one has

$$\left(e_1^i, e_2^j\right) \to \left(\eta e_1^i, \eta^{1/(2-b)}e_2^j\right) \tag{51}$$

where η is a positive constant, $e_1^i, (i = 1, 2, 3)$ is the i-th element of vector $\boldsymbol{e}_1$ and $e_2^j, (j = 1, 2, 3)$ is the j-th element of vector $\boldsymbol{e}_2$, respectively. Thus, the vector space (48) is homogeneous to $(b-1)/(2-b) < 0$. On basis of [36], the finite time stability of closed-loop system (39) is ensured, i.e., the tracking error $\boldsymbol{e}_1$ and $\boldsymbol{e}_2$ would converge to zero in finite time. ■

Remark 3: According to the (38) and (48), the finite-time convergence of the reaching and sliding phase can be guaranteed by the proposed control law. Therefore, the finite-time stability is achieved successfully by the proposed fault tolerant control scheme, which accords with practical demands that the time of accommodation malfunctions for LLV is limited [37].

C. ADP-BASED SUPPLEMENTARY CONTROL DESIGN

In order to improve the tracking performance for LLV and further decrease the tracking errors even existing actuator faults, a supplementary controller is introduced based on the adaptive dynamic programming (ADP) with actor-critic structures [33].

Frist, define the new state as $\boldsymbol{x}(k) = \left[\boldsymbol{e}_1^{\mathrm{T}}(k-1), \boldsymbol{e}_2^{\mathrm{T}}(k-1), \boldsymbol{e}_1^{\mathrm{T}}(k), \boldsymbol{e}_2^{\mathrm{T}}(k)\right]^{\mathrm{T}}$, where $\boldsymbol{e}_1(k-1)$ and $\boldsymbol{e}_2(k-1)$ denote the values of $\boldsymbol{e}_1$ and $\boldsymbol{e}_2$ at previous moment, respectively. k is the discretization step, and Thus, the utility function is given as follows

$$r(\boldsymbol{x}(k), \boldsymbol{u}(k)) = [\boldsymbol{x}^{\mathrm{T}}(k), \boldsymbol{u}^{\mathrm{T}}(k)]\boldsymbol{K}_r[\boldsymbol{x}^{\mathrm{T}}(k), \boldsymbol{u}^{\mathrm{T}}(k)]^{\mathrm{T}} \tag{52}$$

where $\boldsymbol{u}(k) = \boldsymbol{\delta}(k)$ is control input generated by the ADP algorithm, and $\boldsymbol{K}_r$ is a positive-definite diagonal matrix.

Then, the cost function can be formulated as follows

$$J(\boldsymbol{x}(k), \boldsymbol{u}(k)) = \sum_{i=k}^{\infty}\varepsilon^{i-k}r(\boldsymbol{x}(i), \boldsymbol{u}(i)) \tag{53}$$

where $\varepsilon \in (0, 1)$ is the discount factor.

In conclusion, the aim of ADP is to find an appropriate input $\boldsymbol{u}(k)$ which would minimize the cost function

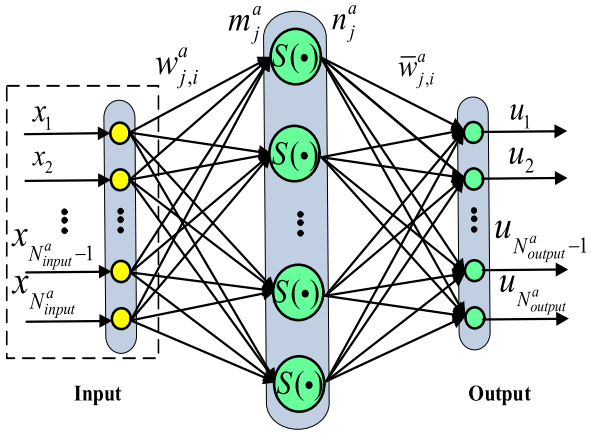

FIGURE 2. The structure of actor networks.

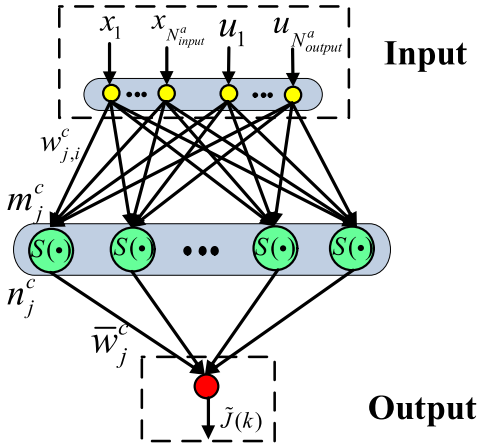

FIGURE 3. The structure of critic networks.

$J(\boldsymbol{x}(t), \boldsymbol{u}(t))$, it follows that

$$J^*(\boldsymbol{x}(k), \boldsymbol{u}(k)) = \min_{\boldsymbol{u}(k)} \sum_{i=k}^{\infty} \varepsilon^{i-k} r(\boldsymbol{x}(i), \boldsymbol{u}(i)) \tag{54}$$

where $J^*(\boldsymbol{x}(t), \boldsymbol{u}(t))$ is the optimal cost function.

According to the optimization theory, we can obtain the following the Bellman equation

$$J^*(\boldsymbol{x}(k), \boldsymbol{u}(k)) = \min_{\boldsymbol{u}(k)} \{r(\boldsymbol{x}(k), \boldsymbol{u}(k)) + \varepsilon J^*(\boldsymbol{x}(k+1), \boldsymbol{u}(k+1))\} \tag{55}$$

Furthermore, the action-critic neural network structure is utilized to get an approximately solution $\tilde{J}(k)$ during the design of supplementary control, and only one hidden layer is employed in the ADP.

Let N^a_{input} and N^a_{output} denote the number of inputs and outputs for action networks, respectively. The input $\boldsymbol{a}_{input}$ and output $\boldsymbol{a}_{output}$ of action networks are described as

$$\boldsymbol{a}_{input} = \boldsymbol{x}(k), \quad \text{and} \quad \boldsymbol{a}_{output} = \boldsymbol{u}(k) \tag{56}$$

And the input $\boldsymbol{c}_{input}$ and output $\boldsymbol{c}_{output}$ of the critic networks can be expressed as

$$\boldsymbol{c}_{input} = \left[\boldsymbol{a}_{input}, \boldsymbol{a}_{output}\right]^{\mathrm{T}}, \quad \text{and} \quad \boldsymbol{c}_{output} = \tilde{J}(k) \tag{57}$$

Then, the number of inputs for critic network is $N^c_{input} = N^a_{input} + N^a_{output}$, and the number of the output is one. The structures of action and critic networks are presented in Figs. 2 and Fig. 3.

For the action networks, the input $m^a_j(k)$ and output $n^a_j(k)$ of the $j-$th node are given as follows

$$m^a_j(k) = \sum_{i=1}^{N^a_{input}} w^a_{j,i}(k) x_i(k), \quad j = 1, 2, \cdots, N^a_h \tag{58}$$

$$n^a_j(k) = S(m^a_j(k)) = \frac{1 - e^{-m^a_j(k)}}{1 + e^{-m^j_a(k)}} \tag{59}$$

where $w^a_{j,i}$ is the weight, the $S(t)$ is a hyperbolic tangent transfer function, i.e. $S(t) = \frac{1-e^{-t}}{1+e^{-t}}$, and N^a_h denotes the number of hidden nodes for action networks. The output $u_p(k)$ of the $p-$th output node can be expressed by

$$u_p(k) = \sum_{j=1}^{N^a_h} \bar{w}^a_{p,j}(k) n^a_j(k), \quad p = 1, 2, \cdots, N^a_o \tag{60}$$

where $\bar{w}^a_{p,j}$ stands for the weights. Define prediction errors as $\boldsymbol{e}_a(k) = \tilde{J}(k) - U_c$, where U_c is the desired ultimate objective function. Then, the prediction error would be back-propagated to train the action networks. Because the objective for the ADP is to make $\boldsymbol{e}_1$ and $\boldsymbol{e}_2$ converge to zero, which implies the $\tilde{J}(k)$ would also be zero. Without loss of generality, let $U_c = 0$, it can be obtained that the error function is $E_a(t) = \frac{\boldsymbol{e}^{\mathrm{T}}_a \boldsymbol{e}_a}{2}$.

Similarly, for the critic networks, the input $m^c_j(k)$ and output $n^c_j(k)$ of the $j-$th hidden node can be described as

$$m^c_j(k) = \sum_{i=1}^{N^a_{input}} w^c_{j,i}(k) x_i(k) + \sum_{i=1}^{N_{ao}} w^c_{j,i+N^a_{input}}(k) u_i(k) \tag{61}$$

$$n^c_j(k) = S\left(m^c_j(k)\right) = \frac{1 - e^{-m^c_j(k)}}{1 + e^{-m^c_j(k)}}, \quad j = 1, 2, \cdots, N_{ch} \tag{62}$$

where $w^c_{j,i}$ represents the weight. And the $\tilde{J}(k)$ is

$$\tilde{J}(k) = \sum_{j=1}^{N^c_{output}} \bar{w}^c_j(k) n^c_j(k) \tag{63}$$

where $\bar{w}^c_j(k)$ is the weight. Define the prediction error as $e_c(k) = \varepsilon \tilde{J}(k) + r(\boldsymbol{x}(k), \boldsymbol{u}(k)) - \tilde{J}(k-1)$, which would be back-propagated to train the critic networks. Thus, the minimum of the error function is $E_c(t) = \frac{1}{2} e^2_c(t)$.

On basis of the gradient descent algorithm, the weight updating policy for action and critic networks are given

as follows:

$$\begin{aligned}
&\Delta w_{j,i}^{a}(k) \\
&= \lambda_a \frac{\partial E_a(k)}{\partial w_{j,i}^{a}(k)} \\
&= -\frac{\lambda_a}{2}\tilde{J}(k) \sum_{p=1}^{N_{output}^{a}} \left[\sum_{l=1}^{N_h^c} \frac{1}{2} \bar{w}_l^c(k) \left(1 - \left(n_l^c(k)\right)^2\right) w_{l,(N_{ai}+p)}^{c} \right] \\
&\quad \cdot \bar{w}_{p,j}^{a}(k) \left(1 - \left(n_j^a(k)\right)^2\right) x_i(k) \qquad (64) \\
&\Delta \bar{w}_{p,j}^{a}(k) \\
&= -\lambda_a \frac{\partial E_a(k)}{\partial \bar{w}_{p,j}^{a}(k)} \\
&= -\frac{\lambda_a}{2}\tilde{J}(k) \left[\sum_{l=1}^{N_h^c} \bar{w}_l^c(k) \left(1 - \left(n_l^c(k)\right)^2\right) w_{l,(N_{ai}+p)}^{c} \right] n_j^a(k) \\
&\qquad (65) \\
&\Delta w_{j,i}^{c}(k) \\
&= -\lambda_c \frac{\partial E_c(k)}{\partial w_{j,i}^{c}(k)} \\
&= -\varepsilon \lambda_c e_c(k) w_j^c(k) \frac{1}{2} \left(1 - \left(n_j^c(k)\right)^2\right) x_i(k) \qquad (66) \\
&\Delta \bar{w}_{j}^{c}(k) \\
&= -\lambda_c \frac{\partial E_c(k)}{\partial \bar{w}_{j}^{c}(k)} = -\varepsilon \lambda_c e_c(k) n_j^c(k) \qquad (67)
\end{aligned}$$

where λ_a and λ_c are learning rates such that $\lambda_a > 0$, $\lambda_c > 0$. Until here, the design of supplementary control scheme based on ADP is completed.

IV. SIMULATION RESULTS

In this section, the numerical simulations are presented to declare the effectiveness of the proposed self-healing control method for the LLV with actuator faults.

The parameters for the LLV on this example are given as: $R = 3.00$ m, $r = 1.00$ m, and $L = 52.00$ m, $x_m = 35.00$ m, $T = 1.2 \times 10^6$ N, $J_{xx} = 2.9 \times 10^6 \text{kg} \cdot \text{m}^2$, and $J_{yy} = J_{zz} = 5.9 \times 10^7 \text{kg} \cdot \text{m}^2$. More information about the launch vehicle can be found in [2] and [21]. The initial states of the attitude system for the LLV are $\boldsymbol{\xi} = [\phi, \psi, \theta]^{\mathrm{T}} = [0, 0, 90°]^{\mathrm{T}}$ and $\omega_x = \omega_y = \omega_z = 0$ deg/s. In addition, the desirable attitude command $\boldsymbol{\xi}_c$ is selected as $\boldsymbol{\xi}_c = [15°, -10°, 80°]^{\mathrm{T}}$. Consider that a desirable attitude constant command $\boldsymbol{\xi}_c$ may bring excessive initial errors, which would produce the huge control input and the peaking value. Thus, a seconded order filter is adopted to smooth the desirable attitude command $\boldsymbol{\xi}_c$, instead of giving the attitude system a constant command directly. The form of the second order filter is given as $G(s) = \frac{0.04}{s^2+0.4s+0.04}$, and the same approach is adopted in [32]. Furthermore, because the measurement noise is an important factor affecting the performance of the control system, the simulation scenario with the measurement noise of angular velocity is also consider in the part. The measurement noise is assumed to be Gauss white noise with mean value of 0 and standard deviation of 0.01.

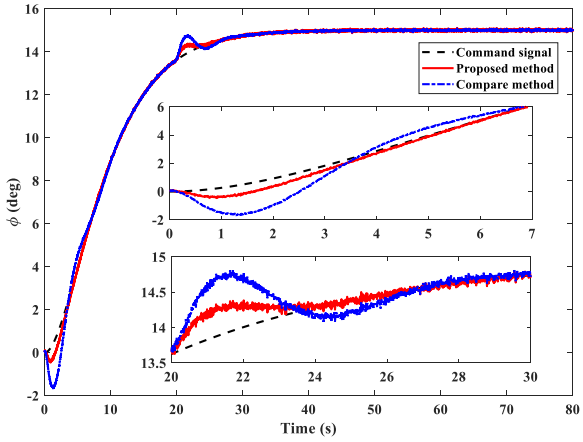

FIGURE 4. The tracking curve of the roll angle.

Considering the energy consumption and the effects of flex-mode and fuel sloshing, the moment of inertia and aerodynamic force/moment coefficients are assumed with 10% uncertainties. The external disturbances $\boldsymbol{d}$ used in this simulation are $\boldsymbol{d} = 10^3 [\sin(t), \cos(t), \sin(t)]^{\mathrm{T}}$ [9]. Furthermore, the following time-varying actuator faults are considered,

$$e_2^{CRE} = \begin{cases} 1 & 0 \le t < 20 \\ 0.65 & 20 \le t, \end{cases} \qquad e_2^{SRE} = \begin{cases} 1 & 0 \le t < 20 \\ 0.7, & 20 \le t \end{cases}$$

$$\rho_3^{CRE} = \begin{cases} 0 & 0 \le t < 20 \\ 100\sin\left(\frac{\pi}{4}t\right) & 20 \le t \end{cases}$$

The parameters for the proposed ESO and self-healing control strategy are selected as: $r_1 = 2.5$, $r_2 = 1$, $r_3 = 8$, $\mu_1 = 0.1$, $\mu_2 = 0.03$, $l_1 = l_2 = 0.75$, $\zeta_1 = 1.25$, $\zeta_2 = 0.5$, $\boldsymbol{K}_r = 0.1 * \boldsymbol{I}$, $\mu = 0.85$. The numbers of the hidden nodes for actor and critic networks are both 12. The initial values of the learning rates are $\lambda_a = \lambda_c = 0.4$, and values of λ_a and λ_c would decrease by 0.05 every ten seconds until $\lambda_a \le 0.005$ and $\lambda_c \le 0.005$. In addition, all the initial weights are in $[-0.35, 0.35]$ randomly, which means that the supplementary magnitude is within a certain degree, and the similar measures are applied in [32] and [33].

By employed the proposed self-healing control strategy to the system (8) for the LLV, the simulation results are given in Figs. 4∼16, from which it can be found that the attitude tracking missions for the LLV are successfully achieved even existing the external disturbances and underside actuator malfunctions. Furthermore, the fault tolerant control methods in [2] are applied in this simulation scenarios as a comparison, and the corresponding results are shown in Figs. 4∼13.

For the bias and part loss of effectiveness malfunctions for the propulsion system, the attitude tracking performances for the LLV with different control schemes are presented in Figs. 4-6. It can be seen that both two control methods could achieve the attitude tracking missions and ensure the stability of the closed-loop system despite actuator failures.

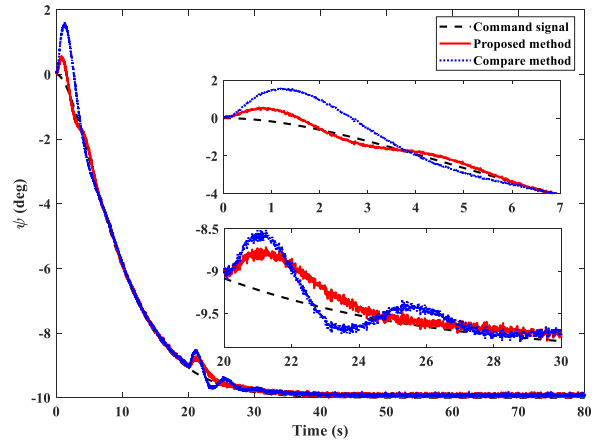

FIGURE 5. The tracking curve of yaw angle.

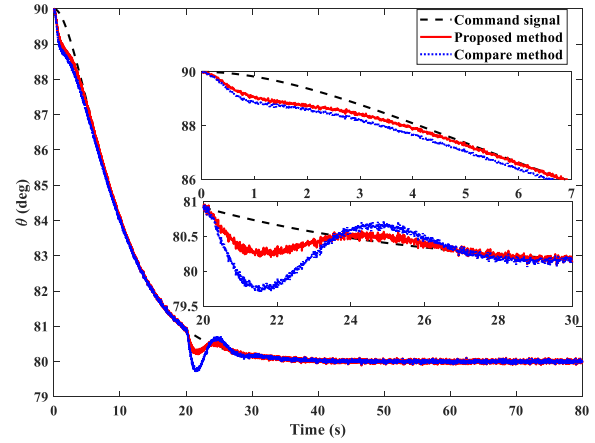

FIGURE 6. The tracking curve of pitch angle.

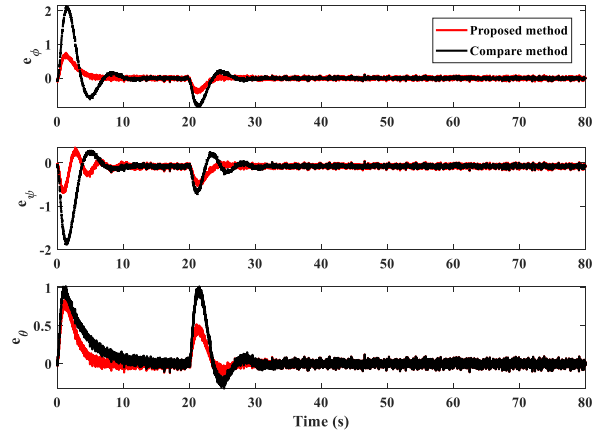

FIGURE 7. The tracking errors of the attitude angle.

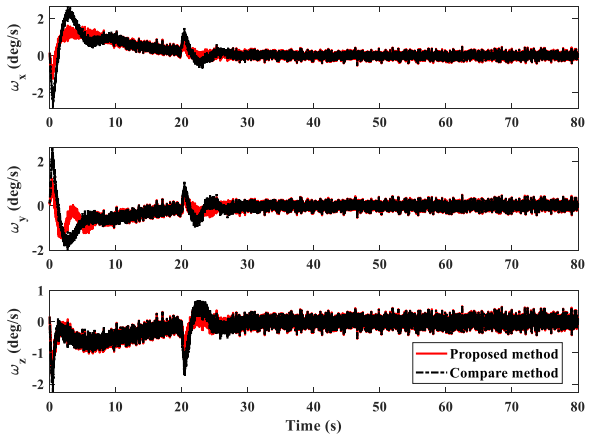

FIGURE 8. The time responses of the attitude velocity.

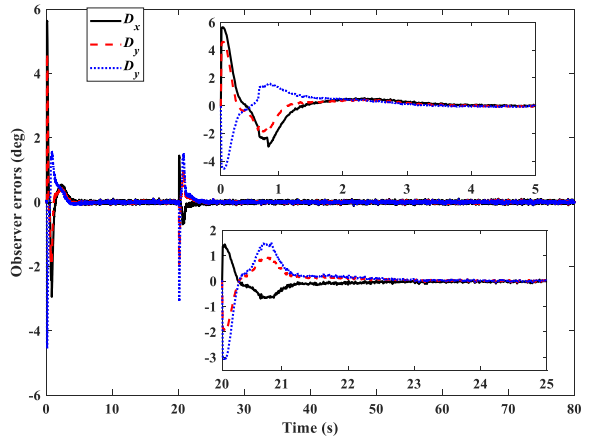

FIGURE 9. The time responses of observer errors.

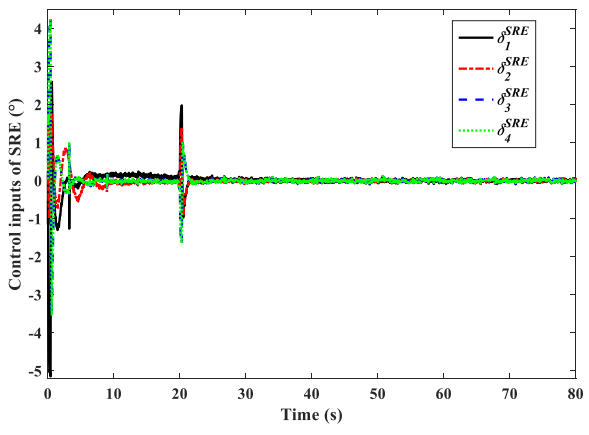

FIGURE 10. Deflection angles of the SRE by proposed methods.

However, a good tracking performance can be guaranteed by the proposed self-healing control in the case of actuator failures. Fig 7 shows the tracking errors of the attitude angle. As we can see from the Fig. 7, a smaller tracking error and shorter convergence time can be obtained by the proposed methods, and the tracking error is less than 0.01 deg. when the undesired malfunctions occur at 20 s, the proposed methods can accommodate the faults faster than the controller in [2]. The time responses of the attitude velocity are depicted in Fig. 8. It is worth mentioning that the closed-loop is stable even in presence of the measurement noise for the angular velocity. an Applying the proposed ESO, the observer error

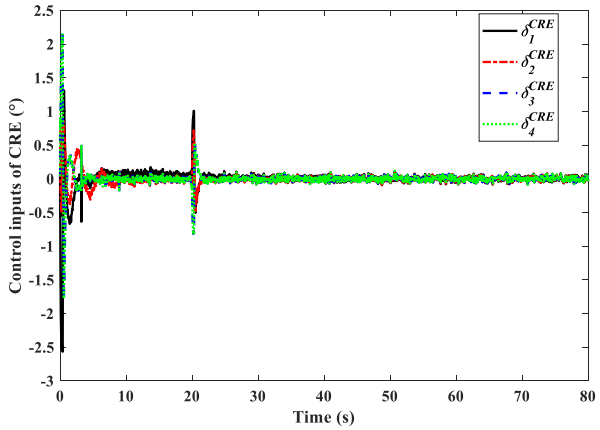

FIGURE 11. Deflection angles of the CRE by proposed methods.

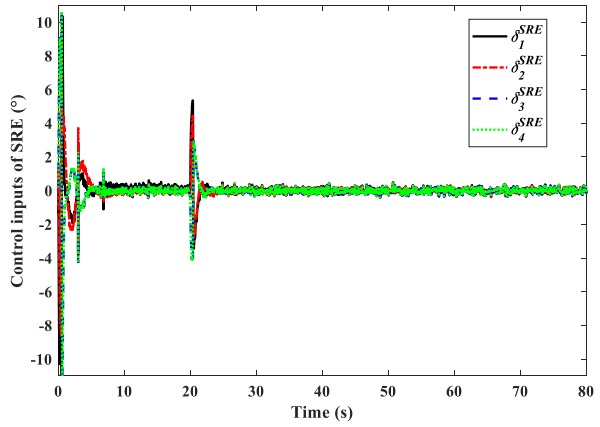

FIGURE 12. Deflection angles of the SRE by methods in [2].

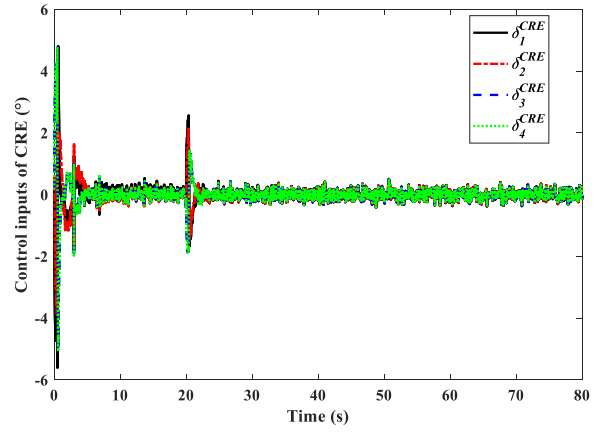

FIGURE 13. Deflection angles of the CRE by methods in [2].

of the compound disturbance $\boldsymbol{D}$ is shown in Fig. 9, from which it can be found that the estimation error would converge to a small region rapidly and the observation error is less than 0.01. It should be pointed that this quality is also guaranteed in the situation with undesired failures.

The deflection angles of the SRE and CRE with two different control methods are given in Figs. 10-13,

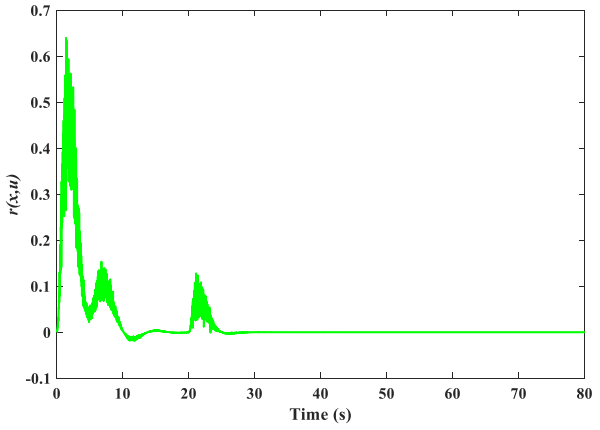

FIGURE 14. The time responses of utility function $r(x, u)$.

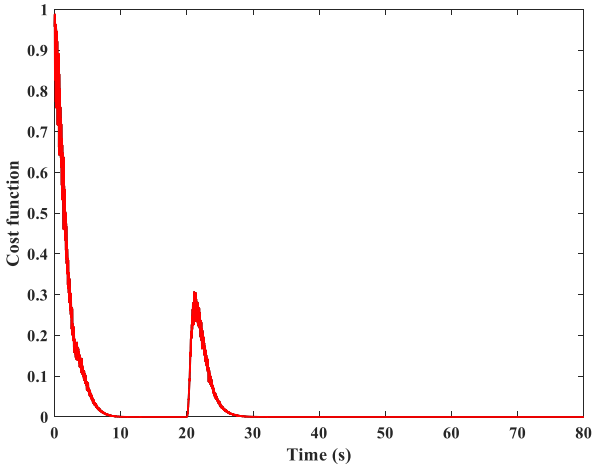

FIGURE 15. The time responses of cost function.

and not larger than ± 12 deg, which satisfy the engineering demand, i.e. the limit of control ability. It can be seen from the Figs. 10-13 that the deflection angles of the SRE by proposed methods change between $+5$ and -5, and the deflection angles of the SRE by [2] change between $+10$ and -10, i.e., there is a smaller region for the control input of the proposed method that [2]. The similar conclusion can be obtained of the deflection angles of the CRE. In addition, the proposed ADP-based supplementary control has a good adaptation and generalization ability for the measurement noise. When the system is stable, the deflection angles of actuators caused by the measurement noise and other external disturbances are in a narrower range than [2].

The utility function $r(\boldsymbol{x}, \boldsymbol{u})$ is represented in Fig 14. It is obvious from Fig. 14 that the utility function would quickly converge to zero when the actuator faults happen at 20 s by the proposed weight updating algorithm, which implies that the attitude tracking error decreases to zero. Fig. 15 shows the curve of cost function, which would converge to zero quickly. Based on proposed supplementary control strategy, the cost function rapidly decreases to zero when the system encounters the malfunctions at 20 s, which further proves the

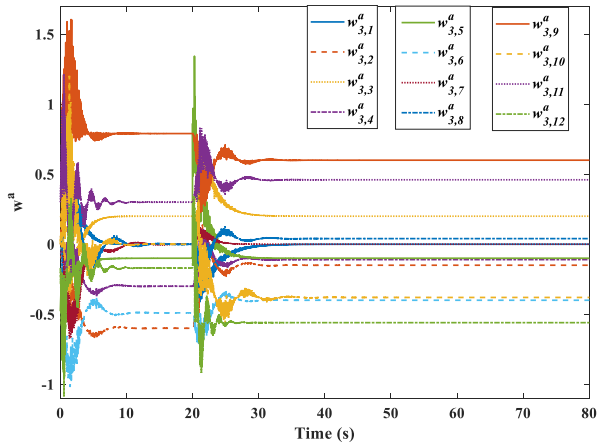

FIGURE 16. The weight updating of w_3^a.

correctness of the proposed methods. Fig. 16 shows weight updating of w_3^a, where the w_3^a denotes the weights from inputs to the third hidden node. As shown in Fig. 16, the weights w_3^a would be adjusted in the simulation process, and converge to certain values. From the above discussions, the simulation results demonstrate the effectiveness and advantage of the control scheme.

V. CONCLUSION

In this note, the self-healing control strategy based on ESO and adaptive dynamic programming is proposed for the attitude system of the LLV. The ESO is first designed to estimate the compound disturbances, including system uncertainties, disturbances, and actuator faults. Specially, the nonlinear gains are applied to reduce the observation errors. Based on the estimations, an integral terminal sliding mode fault tolerant scheme is proposed to ensure the finite-time stability of the closed-loop system even existing malfunctions. Besides, an ADP-based supplementary controller is introduced to further improve the system performance. Finally, the simulations illustrate the effectiveness of the proposed control methods. It should be mentioned that the form of the actuator faults/failures is affine in this paper, and a non-affine form may be considered in the future papers. Furthermore, the fault tolerant control under the actuator saturation is also a significant issue for the LLV, which may be our future research work.

REFERENCES

[1] L. Zhang, C. Wei, R. Wu, and N. Cui, "Fixed-time extended state observer based non-singular fast terminal sliding mode control for a VTVL reusable launch vehicle," *Aerosp. Sci. Technol.*, vols. 82–83, pp. 70–79, Nov. 2018.

[2] D.-J. Zhao, Y.-J. Wang, L. Liu, and Z.-S. Wang, "Robust fault-tolerant control of launch vehicle via GPI observer and integral sliding mode control," *Asian J. Control*, vol. 15, no. 2, pp. 614–623, Mar. 2013.

[3] Q. Mao, L. Dou, Z. Yang, B. Tian, and Q. Zong, "Fuzzy disturbance observer-based adaptive sliding mode control for reusable launch vehicles with aeroservoelastic characteristic," *IEEE Trans Ind. Informat.*, vol. 16, no. 2, pp. 1214–1223, Feb. 2020, doi: 10.1109/TII.2019.2924731.

[4] W. C. A. Kishore, S. Dasgupta, G. Ray, and S. Sen, "Control allocation for an over-actuated satellite launch vehicle," *Aerosp. Sci. Technol.*, vol. 28, no. 1, pp. 56–71, Jul. 2013.

[5] S. Zhao and X. Li, "Prescribed performance fault tolerant control for hypersonic flight vehicles with actuator failures," *IEEE Access*, vol. 7, pp. 100187–100204, Aug. 2019.

[6] D.-J. Zhao and B.-Y. Jiang, "Adaptive fault-tolerant control of heavy lift launch vehicle via differential algebraic observer," *J. Central South Univ.*, vol. 20, no. 8, pp. 2142–2150, Jul. 2013.

[7] A. Casavola, M. Rodrigues, and D. Theilliol, "Self-healing control architectures and design methodologies for linear parameter varying systems," *Int. J. Robust Nonlinear Control*, vol. 25, no. 5, pp. 625–626, Jan. 2015.

[8] H. Xu, D. Wang, C. Liu, W. Li, and F. Fu, "The study on reconfigurability condition of spacecraft control system," *Adv. Astronaut. Sci. Technol.*, vol. 1, no. 2, pp. 197–206, Jan. 2019.

[9] A. Wang, F. Chen, and H. Gong, "Self-healing control for attitude system of hypersonic flight vehicle with body flap faults," *IEEE Access*, vol. 6, pp. 19121–19130, Feb. 2018.

[10] Y. Liu, Z. Ren, and J. E. Cooper, "Integrated strategy for commercial aircraft fault-tolerant control," *J. Guid., Control, Dyn.*, vol. 41, no. 6, pp. 1423–1434, Jun. 2018.

[11] T. Cao, Z. Gao, M. Qian, and J. Zhao, "Passive fault tolerant control approach for hypersonic vehicle with actuator loss of effectiveness faults," in *Proc. Chin. Control Decis. Conf. (CCDC)*, Yinchuan, China, May 2016, pp. 5951–5956.

[12] Q. Shen, D. Wang, S. Zhu, and E. K. Poh, "Integral-type sliding mode fault-tolerant control for attitude stabilization of spacecraft," *IEEE Trans. Control Syst. Technol.*, vol. 23, no. 3, pp. 1131–1138, May 2015.

[13] Q. Shen, D. Wang, S. Zhu, and K. Poh, "Finite-time fault-tolerant attitude stabilization for spacecraft with actuator saturation," *IEEE Trans. Aerosp. Electron. Syst.*, vol. 51, no. 3, pp. 2390–2405, Jul. 2015.

[14] S. Yin, B. Xiao, S. X. Ding, and D. Zhou, "A review on recent development of spacecraft attitude fault tolerant control system," *IEEE Trans. Ind. Electron.*, vol. 63, no. 5, pp. 3311–3320, May 2016.

[15] X. Liang, Q. Wang, C. Hu, and C. Dong, "Observer-based H_∞ fault-tolerant attitude control for satellite with actuator and sensor faults," *Aerosp. Sci. Technol.*, vol. 95, Dec. 2019, Art. no. 105424, doi: 10.1016/j.ast.2019.105424.

[16] M. Ran, Q. Wang, and C. Dong, "Active disturbance rejection control for uncertain nonaffine-in-control nonlinear systems," *IEEE Trans. Autom. Control*, vol. 62, no. 11, pp. 5830–5836, Nov. 2017.

[17] Z. Liu, S. Liu, Z. Li, and I. A. Tasiu, "A novel approach based on extended state observer sliding mode control to suppress voltage low frequency oscillation of traction network," *IEEE Access*, vol. 7, pp. 52440–52454, Apr. 2019.

[18] B. Li, Q. Hu, Y. Yu, and G. Ma, "Observer-based fault-tolerant attitude control for rigid spacecraft," *IEEE Trans. Aerosp. Electron. Syst.*, vol. 53, no. 5, pp. 2572–2582, Oct. 2017.

[19] D. Aravindh, R. Sakthivel, B. Kaviarasan, S. M. Anthoni, and F. Alzahrani, "Design of observer-based non-fragile load frequency control for power systems with electric vehicles," *ISA Trans.*, vol. 91, pp. 21–31, Aug. 2019.

[20] Y. Liu, Q. Wang, C. Hu, and C. Dong, "ESO-based fault-tolerant anti-disturbance control for air-breathing hypersonic vehicles with variable geometry inlet," *Nonlinear Dyn.*, vol. 98, no. 3, pp. 2293–2308, Nov. 2019.

[21] L. Zhang, C. Wei, R. Wu, and N. Cui, "Adaptive fault-tolerant control for a VTVL reusable launch vehicle," *Acta Astronautica*, vol. 159, pp. 362–370, Jun. 2019.

[22] R. Sakthivel, S. Mohanapriya, B. Kaviarasan, Y. Ren, and S. M. Anthoni, "Non-fragile control design and state estimation for vehicle dynamics subject to input delay and actuator faults," *IET Control Theory Appl.*, vol. 14, no. 1, pp. 134–144, Jan. 2020.

[23] R. Mu, J. Chen, K. Peng, X. Zhang, Y. Deng, and N. Cui, "Finite-time super-twisting controller based on SESO design for RLV re-entry phase," *IEEE Access*, vol. 7, pp. 37371–37380, Apr. 2019.

[24] X. Qi, D. Theilliol, J. Qi, Y. Zhang, L. Wang, and J. Han, "Self healing control method against unmanned helicopter actuator stuck faults," in *Proc. Int. Conf. Unmanned Aircr. Syst. (ICUAS)*, Orlando, FL, USA, May 2014, pp. 842–847.

[25] M. Zhou, Z. Wang, D. Theilliol, Y. Shen, and M. Rodrigues, "A self-healing control method for satellite attitude tracking based on simultaneous fault estimation and control design," in *Proc. 3rd Conf. Control Fault-Tolerant Syst. (SysTol)*, Barcelona, Spain, Sep. 2016, pp. 349–354.

[26] D. P. Bertsekas, "Value and policy iterations in optimal control and adaptive dynamic programming," *IEEE Trans. Neural Netw. Learn. Syst.*, vol. 28, no. 3, pp. 500–509, Mar. 2017.

[27] A. Heydari, "Theoretical and numerical analysis of approximate dynamic programming with approximation errors," *J. Guid., Control, Dyn.*, vol. 39, no. 2, pp. 301–311, Feb. 2016.
[28] T. Bian, Y. Jiang, and Z.-P. Jiang, "Adaptive dynamic programming and optimal control of nonlinear nonaffine systems," *Automatica*, vol. 50, no. 10, pp. 2624–2632, Oct. 2014.
[29] B. Zhao, D. Liu, X. Yang, and Y. Li, "Observer-critic structure-based adaptive dynamic programming for decentralised tracking control of unknown large-scale nonlinear systems," *Int. J. Syst. Sci.*, vol. 48, no. 9, pp. 1978–1989, Mar. 2017.
[30] Y. Zhou, E.-J.-V. Kampen, and Q. Chu, "Nonlinear adaptive flight control using incremental approximate dynamic programming and output feedback," *J. Guid., Control, Dyn.*, vol. 40, no. 2, pp. 493–500, Feb. 2017.
[31] C. Mu, Z. Ni, C. Sun, and H. He, "Air-breathing hypersonic vehicle tracking control based on adaptive dynamic programming," *IEEE Trans. Neural Netw. Learn. Syst.*, vol. 28, no. 3, pp. 584–598, Mar. 2017.
[32] L. Gong, Q. Wang, and C. Dong, "Disturbance rejection control of morphing aircraft based on switched nonlinear systems," *Nonlinear Dyn.*, vol. 96, no. 2, pp. 975–995, Feb. 2019.
[33] L.-G. Gong, Q. Wang, and C.-Y. Dong, "Spacecraft output feedback attitude control based on extended state observer and adaptive dynamic programming," *J. Franklin Inst.*, vol. 356, no. 10, pp. 4971–5000, Jul. 2019.
[34] Q. Dong, Q. Zong, B. Tian, C. Zhang, and W. Liu, "Adaptive disturbance observer-based finite-time continuous fault-tolerant control for reentry RLV," *Int. J. Robust Nonlinear Control*, vol. 27, no. 18, pp. 4275–4295, Mar. 2017.
[35] A. Chalanga, S. Kamal, L. M. Fridman, B. Bandyopadhyay, and J. A. Moreno, "Implementation of super-twisting control: Supper-twisting and higher oeder sliding-mode observer-based approaches," *IEEE Trans. Ind. Informat.*, vol. 63, no. 6, pp. 3677–3685, Jun. 2016.
[36] S. Bhat and D. Bernstein, "Finite-time stability of continous autonomous systems," *SIAM J. Control Optim.*, vol. 38, no. 3, pp. 751–766, Feb. 2000.
[37] X. Yu, P. Li, and Y. Zhang, "The design of fixed-time observer and finite-time fault-tolerant control for hypersonic gliding vehicles," *IEEE Trans. Ind. Electron.*, vol. 65, no. 5, pp. 4135–4144, May 2018.
[38] C. Liu, G. Vukovich, Z. Sun, and K. Shi, "Observer-based fault-tolerant attitude control for spacecraft with input delay," *J. Guid., Control, Dyn.*, vol. 41, no. 9, pp. 2041–2053, Sep. 2018.

XIAOHUI LIANG received the B.Eng. degree in automation control from Northwestern Polytechnical University, Xi'an, China, in 2004. He is currently pursuing the Ph.D. degree in control science and engineering with the School of Automation Science and Electrical Engineering, Beihang University, Beijing, China. His research interests include the fault tolerant control in aircrafts, active disturbance rejection control techniques, and reinforcement learning.

QING WANG received the Ph.D. degree in control engineering from Northwestern Polytechnic University, Xi'an, in 1996. She is currently a Professor with the School of Automation Science and Electrical Engineering, Beihang University, Beijing, China. She has published four books and authored or coauthored approximately 80 articles in the field of flight control. Her current research interests include aircraft intelligent control, fault tolerant control, and switch control.

CHANGHUA HU received the B.Eng. degree in control science and engineering and the M.Eng. degree in instrument science and technology from the High-Tech Institute of Xi'an, Xi'an, China, in 1987 and 1990, respectively, and the Ph.D. degree from Northwestern Polytechnic University, Xi'an, in 1996. In 2008, he was a Visiting Scholar with the University of Duisburg-Essen, Essen, Germany, from September 2008 to December 2008. He is currently a Professor with the High-Tech Institute of Xi'an. He has published two books and about 100 articles. His current research interests include fault diagnosis and prediction, life prognosis, and fault-tolerant control.

ZHIJIE ZHOU received the B.Eng. and M.Eng. degrees from the High-Tech Institute of Xi'an, Xi'an, China, in 2001 and 2004, respectively, and the Ph.D. degree from Tsinghua University, Beijing, China, in 2010, all in control science and management. In 2009, he was a Visiting Scholar with The University of Manchester, Manchester, U.K., for six months. He is currently an Associate Professor with the High-Tech Institute of Xi'an. He has published about 70 articles. His research interests include belief rule-base, dynamic system modeling, hybrid quantitative and qualitative decision modeling, and the fault prognosis and optimal maintenance of dynamic systems.

CONG FENG received the B.Eng. degree in control engineering from Beihang University, Beijing, China, in 2014, where he is currently pursuing the Ph.D. degree in control science and engineering with the School of Automation Science and Electrical Engineering. His research interests include morphing wing aircraft control, active disturbance rejection control techniques, and deep reinforcement learning.